

GW170104: Observation of a 50-Solar-Mass Binary Black Hole Coalescence at Redshift 0.2

The LIGO Scientific Collaboration and the Virgo Collaboration

We describe the observation of GW170104, a gravitational-wave signal produced by the coalescence of a pair of stellar-mass black holes. The signal was measured on January 4, 2017 at 10:11:58.6 UTC by the twin advanced detectors of the Laser Interferometer Gravitational-Wave Observatory during their second observing run, with a network signal-to-noise ratio of 13 and a false alarm rate less than 1 in 70,000 years. The inferred component black hole masses are $31.2^{+8.4}_{-6.0} M_{\odot}$ and $19.4^{+5.3}_{-5.9} M_{\odot}$ (at the 90% credible level). The black hole spins are best constrained through measurement of the effective inspiral spin parameter, a mass-weighted combination of the spin components perpendicular to the orbital plane, $\chi_{\text{eff}} = -0.12^{+0.21}_{-0.30}$. This result implies that spin configurations with both component spins positively aligned with the orbital angular momentum are disfavored. The source luminosity distance is 880^{+450}_{-390} Mpc corresponding to a redshift of $z = 0.18^{+0.08}_{-0.07}$. We constrain the magnitude of modifications to the gravitational-wave dispersion relation and perform null tests of general relativity. Assuming that gravitons are dispersed in vacuum like massive particles, we bound the graviton mass to $m_g \leq 7.7 \times 10^{-23} \text{ eV}/c^2$. In all cases, we find that GW170104 is consistent with general relativity.

I. INTRODUCTION

The first observing run of the Advanced Laser Interferometer Gravitational-Wave Observatory (LIGO) [1] identified two binary black hole coalescence signals with high statistical significance, GW150914 [2] and GW151226 [3], as well as a less significant candidate LVT151012 [4, 5]. These discoveries ushered in a new era of observational astronomy, allowing us to investigate the astrophysics of binary black holes and test general relativity (GR) in ways that were previously inaccessible [6, 7]. We now know that there is a population of binary black holes with component masses $\gtrsim 25 M_{\odot}$ [5, 6], and that merger rates are high enough for us to expect more detections [5, 8].

Advanced LIGO’s second observing run began on November 30, 2016. On January 4, 2017, a gravitational-wave signal was detected with high statistical significance. Figure 1 shows a time–frequency representation of the data from the LIGO Hanford and Livingston detectors, with the signal GW170104 visible as the characteristic chirp of a binary coalescence. Detailed analyses demonstrate that GW170104 arrived at Hanford ~ 3 ms before Livingston, and originated from the coalescence of two stellar-mass black holes at a luminosity distance of ~ 3 billion light-years.

GW170104’s source is a heavy binary black hole system, with a total mass of $\sim 50 M_{\odot}$, suggesting formation in a sub-solar metallicity environment [6]. Measurements of the black hole spins show a preference away from being (positively) aligned with the orbital angular momentum, but do not exclude zero spins. This is distinct from the case for GW151226, which had a strong preference for spins with positive projections along the orbital angular momentum [3]. The inferred merger rate agrees with previous calculations [5, 8], and could potentially be explained by binary black holes forming through isolated binary evolution or dynamical interactions in dense stellar clusters [6].

Gravitational-wave observations of binary black holes are the ideal means to test GR and its alternatives. They provide insight into regimes of strong-field gravity where velocities are relativistic and the spacetime is dynamic. The tests performed with the sources detected in the first observing run showed no evidence of departure from GR’s predictions [5, 7]; GW170104 provides an opportunity to tighten these constraints. In addition to repeating tests performed in the first observing run, we also test for modifications to the gravitational-wave dispersion relation. Combining measurements from GW170104 with our previous results, we obtain new gravitational-wave constraints on potential deviations from GR.

II. DETECTORS AND DATA QUALITY

The LIGO detectors measure gravitational-wave strain using two dual-recycled Fabry–Perot Michelson interferometers at the Hanford and Livingston observatories [1, 10]. After the first observing run, both LIGO detectors underwent commissioning to reduce instrumental noise, and to improve duty factor and data quality (see Appendix A in the *Supplemental Material* [11]). For the Hanford detector, a high-power laser stage was introduced, and as the first step the laser power was increased from 22 W to 30 W to reduce shot noise [10] at high frequencies. For the Livingston detector, the laser power was unchanged, but there was a significant improvement in low-frequency performance mainly due to the mitigation of scattered light noise.

Calibration of the interferometers is performed by inducing test-mass motion using photon pressure from modulated calibration lasers [12, 13]. The one-sigma calibration uncertainties for strain data in both detectors for the times used in this analysis are better than 5% in amplitude and 3° in phase over the frequency range 20–1024 Hz.

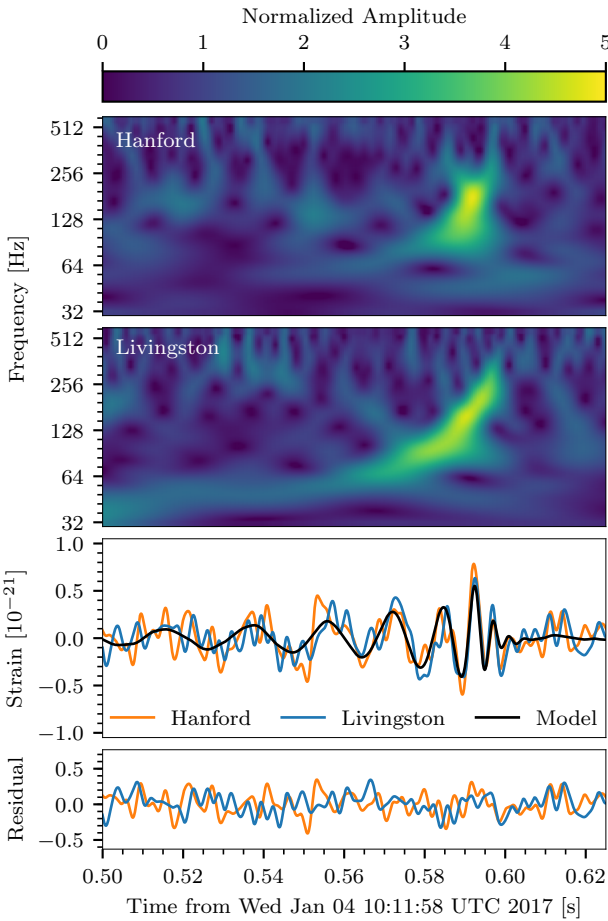


FIG. 1. Time–frequency representation [9] of strain data from Hanford and Livingston detectors (top two panels) at the time of GW170104. The data begin at 1167559936.5 GPS time. The third panel from top shows the time-series data from each detector with a 30–350 Hz bandpass filter, and band-reject filters to suppress strong instrumental spectral lines. The Livingston data have been shifted back by 3 ms to account for the source’s sky location, and the sign of its amplitude has been inverted to account for the detectors’ different orientations. The maximum-likelihood binary black hole waveform given by the full-precession model (see Sec. IV) is shown in black. The bottom panel shows the residuals between each data stream and the maximum-likelihood waveform.

At the time of GW170104, both LIGO detectors were operating with sensitivity typical of the observing run to date and were in an observation-ready state. Investigations similar to the detection validation procedures for previous events [2, 14] found no evidence that instrumental or environmental disturbances contributed to GW170104.

III. SEARCHES

GW170104 was first identified by inspection of low-latency triggers from Livingston data [15–17]. An automated notification was not generated as the Hanford detector’s calibration state was temporarily set incorrectly in the low-latency system. After it was manually determined that the calibration of both detectors was in a nominal state, an alert with an initial source localization [18, 19] was distributed to collaborating astronomers [20] for the purpose of searching for a transient counterpart. Twenty-eight groups of observers covered the parts of the sky localization using ground- and space-based instruments, spanning from γ ray to radio frequencies as well as high-energy neutrinos [21].

Offline analyses are used to determine the significance of candidate events. They benefit from improved calibration and refined data quality information that is unavailable to low-latency analyses [5, 14]. The second observing run is divided into periods of two-detector coincident observing time with $\gtrsim 5$ days of data to measure the false alarm rate of the search at the level where detections can be confidently claimed. Two independently designed matched filter analyses [16, 22] used 5.5 days of coincident data collected from January 4, 2017 to January 22, 2017.

These analyses search for binary coalescences over a range of possible masses and by using discrete banks [23–28] of waveform templates modeling binaries with component spins aligned or antialigned with the orbital angular momentum [29]. The searches can target binary black hole mergers with detector-frame total masses $2 M_{\odot} \leq M^{\text{det}} \lesssim 100\text{--}500 M_{\odot}$, and spin magnitudes up to ~ 0.99 . The upper mass boundary of the bank is determined by imposing a lower limit on the duration of the template in the detectors’ sensitive frequency band [30]. Candidate events must be found in both detectors by the same template within 15 ms [4]. This 15-ms window is determined by the 10-ms intersite propagation time plus an allowance for the uncertainty in identified signal arrival times of weak signals. Candidate events are assigned a detection statistic value ranking their relative likelihood of being a gravitational-wave signal: the search uses an improved detection statistic compared to the first observing run [31]. The significance of a candidate event is calculated by comparing its detection statistic value to an estimate of the background noise [4, 16, 17, 22]. GW170104 was detected with a network matched-filter signal-to-noise ratio (SNR) of 13. At the detection statistic value assigned to GW170104, the false alarm rate is less than 1 in 70,000 years of coincident observing time.

The probability of astrophysical origin P_{astro} for a candidate event is found by comparing the candidate’s detection statistic to a model described by the distributions and rates of both background and signal events [8, 32, 33]. The background distribution is analysis dependent, being derived from the background samples used to calculate the false alarm rate. The signal distribution can depend

on the mass distribution of the source systems; however, we find that different models of the binary black hole mass distribution (as described in Sec. VI) lead to negligible differences in the resulting value of P_{astro} . At the detection statistic value of GW170104, the background rate in both matched filter analyses is dwarfed by the signal rate, yielding $P_{\text{astro}} > 1 - (3 \times 10^{-5})$.

An independent analysis that is not based on matched filtering, but instead looks for generic gravitational-wave bursts [2, 34] and selects events where the signal frequency rises over time [35], also identified GW170104. This approach allows for signal deviations from the waveform models used for matched filtering at the cost of a lower significance for signals that are represented by the considered templates. This analysis reports a false alarm rate of ~ 1 in 20,000 years for GW170104.

IV. SOURCE PROPERTIES

The source parameters are inferred from a coherent Bayesian analysis of the data from both detectors [36, 37]. As a cross-check, we use two independent model-waveform families. Both are tuned to numerical-relativity simulations of binary black holes with non-precessing spins, and introduce precession effects through approximate prescriptions. One model includes inspiral spin precession using a single effective spin parameter χ_p [38–40]; the other includes the generic two-spin inspiral precession dynamics [41–43]. We refer to these as the effective-precession and full-precession models, respectively [44]. The two models yield consistent results. Table I shows selected source parameters for GW170104; unless otherwise noted, we quote the median and symmetric 90% credible interval for inferred quantities. The final mass (or equivalently the energy radiated), final spin and peak luminosity are computed using averages of fits to numerical-relativity results [45–49]. The parameter uncertainties include statistical and systematic errors from averaging posterior probability distributions over the two waveform models, as well as calibration uncertainty [37] (and systematic uncertainty in the fit for peak luminosity). Statistical uncertainty dominates the overall uncertainty as a consequence of the moderate SNR.

For binary coalescences, the gravitational-wave frequency evolution is primarily determined by the component masses. For higher mass binaries, merger and ring-down dominate the signal, allowing good measurements of the total mass $M = m_1 + m_2$ [53–57]. For lower mass binaries, like GW151226 [3], the inspiral is more important, providing precision measurements of the chirp mass $\mathcal{M} = (m_1 m_2)^{3/5} / M^{1/5}$ [58–61]. The transition between the regimes depends upon the detectors' sensitivity, and GW170104 sits between the two. The inferred component masses are shown in Fig. 2. The form of the two-dimensional distribution is guided by the combination of constraints on M and \mathcal{M} . The binary was composed of two black holes with masses $m_1 = 31.2_{-6.0}^{+8.4} M_\odot$ and

TABLE I. Source properties for GW170104: median values with 90% credible intervals. We quote source-frame masses; to convert to the detector frame, multiply by $(1+z)$ [50, 51]. The redshift assumes a flat cosmology with Hubble parameter $H_0 = 67.9 \text{ km s}^{-1} \text{ Mpc}^{-1}$ and matter density parameter $\Omega_m = 0.3065$ [52]. More source properties are given in Table II in the *Supplemental Material* [11].

| | |
|---|---|
| Primary black hole mass m_1 | $31.2_{-6.0}^{+8.4} M_\odot$ |
| Secondary black hole mass m_2 | $19.4_{-5.9}^{+5.3} M_\odot$ |
| Chirp mass \mathcal{M} | $21.1_{-2.7}^{+2.4} M_\odot$ |
| Total mass M | $50.7_{-5.0}^{+5.9} M_\odot$ |
| Final black hole mass M_f | $48.7_{-4.6}^{+5.7} M_\odot$ |
| Radiated energy E_{rad} | $2.0_{-0.7}^{+0.6} M_\odot c^2$ |
| Peak luminosity ℓ_{peak} | $3.1_{-1.3}^{+0.7} \times 10^{56} \text{ erg s}^{-1}$ |
| Effective inspiral spin parameter χ_{eff} | $-0.12_{-0.30}^{+0.21}$ |
| Final black hole spin a_f | $0.64_{-0.20}^{+0.09}$ |
| Luminosity distance D_L | $880_{-390}^{+450} \text{ Mpc}$ |
| Source redshift z | $0.18_{-0.07}^{+0.08}$ |

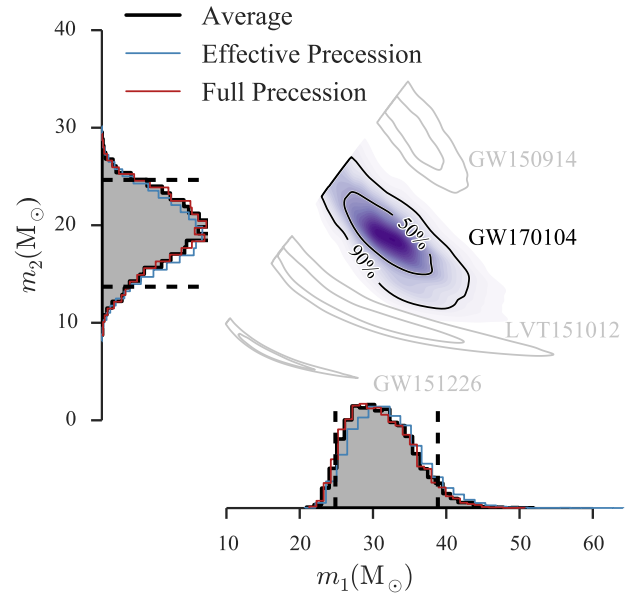


FIG. 2. Posterior probability density for the source-frame masses m_1 and m_2 (with $m_1 \geq m_2$). The one-dimensional distributions include the posteriors for the two waveform models, and their average (black). The dashed lines mark the 90% credible interval for the average posterior. The two-dimensional plot shows the contours of the 50% and 90% credible regions plotted over a color-coded posterior density function. For comparison, we also show the two-dimensional contours for the previous events [5].

$m_2 = 19.4^{+5.3}_{-5.9} M_\odot$; these merged into a final black hole of mass $48.7^{+5.7}_{-4.6} M_\odot$. This binary ranks second, behind GW150914's source [5, 37], as the most massive stellar-mass binary black hole system observed to date.

The black hole spins play a subdominant role in the orbital evolution of the binary, and are more difficult to determine. The orientations of the spins evolve due to precession [62, 63], and we report results at a point in the inspiral corresponding to a gravitational-wave frequency of 20 Hz [37]. The effective inspiral spin parameter $\chi_{\text{eff}} = (m_1 a_1 \cos \theta_{LS_1} + m_2 a_2 \cos \theta_{LS_2})/M$ is the most important spin combination for setting the properties of the inspiral [64–66] and remains important through to merger [67–71]; it is approximately constant throughout the orbital evolution [72, 73]. Here $\theta_{LS_i} = \cos^{-1}(\hat{\mathbf{L}} \cdot \hat{\mathbf{S}}_i)$ is the tilt angle between the spin \mathbf{S}_i and the orbital angular momentum \mathbf{L} , which ranges from 0° (spin aligned with orbital angular momentum) to 180° (spin antialigned); $a_i = |\mathbf{cS}_i/Gm_i^2|$ is the (dimensionless) spin magnitude, which ranges from 0 to 1, and $i = 1$ for the primary black hole and $i = 2$ for the secondary. We use the Newtonian angular momentum for \mathbf{L} , such that it is normal to the orbital plane; the total orbital angular momentum differs from this because of post-Newtonian corrections. We infer that $\chi_{\text{eff}} = -0.12^{+0.21}_{-0.30}$. Similarly to GW150914 [5, 37, 44], χ_{eff} is close to zero with a preference towards being negative: the probability that $\chi_{\text{eff}} < 0$ is 0.82. Our measurements therefore disfavor a large total spin positively aligned with the orbital angular momentum, but do not exclude zero spins.

The in-plane components of the spin control the amount of precession of the orbit [62]. This may be quantified by the effective precession spin parameter χ_p which ranges from 0 (no precession) to 1 (maximal precession) [39]. Figure 3 (top) shows the posterior probability density for χ_{eff} and χ_p [39]. We gain some information on χ_{eff} , excluding large positive values, but, as for previous events [3, 5, 37], the χ_p posterior is dominated by the prior (see Appendix C in the *Supplemental Material* [11]). No meaningful constraints can be placed on the magnitudes of the in-plane spin components and hence precession.

The inferred component spin magnitudes and orientations are shown in Fig. 3 (bottom). The lack of constraints on the in-plane spin components means that we learn almost nothing about the spin magnitudes. The secondary's spin is less well constrained as the less massive component has a smaller impact on the signal. The probability that the tilt θ_{LS_i} is less than 45° is 0.04 for the primary black hole and 0.08 for the secondary, whereas the prior probability is 0.15 for each. Considering the two spins together, the probability that both tilt angles are less than 90° is 0.05. Effectively all of the information comes from constraints on χ_{eff} combined with the mass ratio (and our prior of isotropically distributed orientations and uniformly distributed magnitudes) [5].

The source's luminosity distance D_L is inferred from the signal amplitude [37, 74]. The amplitude is inversely

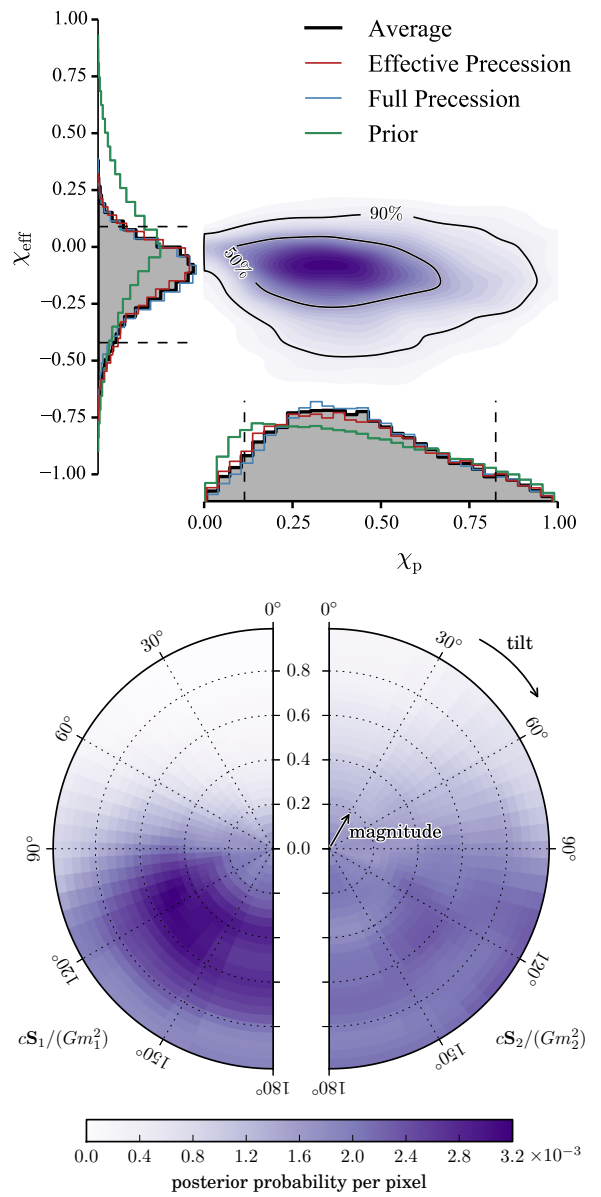


FIG. 3. *Top:* Posterior probability density for the effective inspiral and precession spin parameters, χ_{eff} and χ_p . The one-dimensional distributions show the posteriors for the two waveform models, their average (black), and the prior distributions (green). The dashed lines mark the 90% credible interval for the average posterior. The two-dimensional plot shows the 50% and 90% credible regions plotted over the posterior density function. *Bottom:* Posterior probabilities for the dimensionless component spins, $c\mathbf{S}_1/(Gm_1^2)$ and $c\mathbf{S}_2/(Gm_2^2)$, relative to the normal of the orbital plane $\hat{\mathbf{L}}$. The tilt angles are 0° for spins aligned with the orbital angular momentum and 180° for spins antialigned. The probabilities are marginalized over the azimuthal angles. The pixels have equal prior probability (1.6×10^{-3}); they are spaced linearly in spin magnitudes and the cosine of the tilt angles. Results are given at a gravitational-wave frequency of 20 Hz.

proportional to the distance, but also depends upon the binary's inclination [59, 75–77]. This degeneracy is a significant source of uncertainty [57, 71]. The inclination has a bimodal distribution with broad peaks for face-on and face-off orientations (see Fig. 9 if the *Supplemental Material* [11]). GW170104's source is at $D_L = 880^{+450}_{-390}$ Mpc, corresponding to a cosmological redshift of $z = 0.18^{+0.08}_{-0.07}$ [52]. While GW170104's source has masses and spins comparable to GW150914's, it is most probably at a greater distance [5, 37].

For GW150914, extensive studies were made to verify the accuracy of the model waveforms for parameter estimation through comparisons with numerical-relativity waveforms [78, 79]. GW170104 is a similar system to GW150914 and, therefore, it is unlikely that there are any significant biases in our results as a consequence of waveform modeling. The lower SNR of GW170104 makes additional effects not incorporated in the waveform models, such as higher modes [55, 80, 81], less important. However, if the source is edge on or strongly precessing, there could be significant biases in quantities including \mathcal{M} and χ_{eff} [78]. Comparison to numerical-relativity simulations of binary black holes with non-precessing spins [79], including those designed to replicate GW170104, produced results (and residuals) consistent with the model-waveform analysis.

V. WAVEFORM RECONSTRUCTIONS

Consistency of GW170104 with binary black hole waveform models can also be explored through comparisons with a morphology-independent signal model [82]. We choose to describe the signal as a superposition of an arbitrary number of Morlet–Gabor wavelets, which models an elliptically polarized, coherent signal in the detector network. Figure 4 plots whitened detector data at the time of GW170104, together with waveforms drawn from the 90% credible region of the posterior distributions of the morphology-independent model and the binary black hole waveform models used to infer the source properties. The signal appears in the two detectors with slightly different amplitudes, and a relative phase shift of approximately 180° , because of their different spatial orientations [2]. The wavelet- and template-based reconstructions differ at early times because the wavelet basis requires high-amplitude, well-localized signal energy to justify the presence of additional wavelets, while the earlier portion of the signal is inherently included in the binary black hole waveform model.

The waveforms reconstructed from the morphology-independent model are consistent with the characteristic inspiral–merger–ringdown structure. The overlap [58] between the maximum-likelihood waveform of the binary black hole model and the median waveform of the morphology-independent analysis is 87%, consistent with expectations from Monte Carlo analysis of binary black hole signals injected into detector data [34]. We also

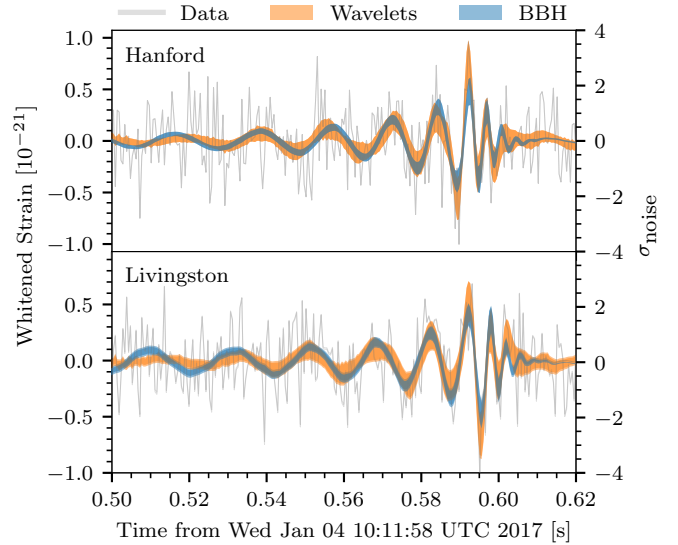


FIG. 4. Time-domain detector data (gray), and 90% confidence intervals for waveforms reconstructed from the morphology-independent wavelet analysis (orange) and binary black hole (BBH) models from both waveform families (blue), whitened by each instrument's noise amplitude spectral density. The left ordinate axes are normalized such that the amplitude of the whitened data and the physical strain are equal at 200 Hz. The right ordinate axes are in units of noise standard deviations. The width of the BBH region is dominated by the uncertainty in the astrophysical parameters.

use the morphology-independent analysis to search for residual gravitational-wave energy after subtracting the maximum-likelihood binary black hole signal from the measured strain data. There is an 83% posterior probability in favor of Gaussian noise versus residual coherent gravitational-wave energy which is not described by the waveform model, implying that GW170104's source is a black hole binary.

VI. BINARY BLACK HOLE POPULATIONS AND MERGER RATES

The addition of the first 11 days of coincident observing time in the second observing run, and the detection of GW170104, leads to an improved estimate of the rate density of binary black hole mergers. We adopt two simple representative astrophysical population models: a distribution that is a power law in m_1 and uniform in m_2 , $p(m_1, m_2) \propto m_1^{-\alpha} / (m_1 - 5 M_\odot)$ with $\alpha = 2.35$ [83], and a distribution uniform in the logarithm of each of the component masses [5, 8]. In both cases, we impose $m_1, m_2 \geq 5 M_\odot$ and $M \leq 100 M_\odot$ [8]. Using the results from the first observing run as a prior, we obtain updated rates estimates of $R = 103^{+110}_{-63}$ Gpc $^{-3}$ yr $^{-1}$ for the power law, and $R = 32^{+33}_{-20}$ Gpc $^{-3}$ yr $^{-1}$ for the

uniform-in-log distribution [5]. These combine search results from the two offline matched filter analyses, and marginalize over the calibration uncertainty [32]. The range for the merger rate that brackets the two distributions, $12\text{--}213 \text{ Gpc}^{-3} \text{ yr}^{-1}$, is consistent with the range $9\text{--}240 \text{ Gpc}^{-3} \text{ yr}^{-1}$ estimated from the first observing run [5, 8]. Recalculating the rates directly after observing a new event can bias rate estimates, but this bias decreases with increasing event count and is negligible compared to other uncertainties on the intervals. While the median estimates have not changed appreciably, the overall tightening in the credible intervals is consistent with the additional observation time and the increment in the number of events with significant probability of being astrophysical from 3 to 4.

Following the first observing run, we performed a hierarchical analysis using the inferred masses of GW150914, LVT151012 and GW151226 to constrain the binary black hole mass distribution. We assumed the power-law population distribution described above, treating α as a parameter to be estimated, and found $\alpha = 2.5^{+1.5}_{-1.6}$ [5]. With the addition of GW170104, α is estimated to be $2.3^{+1.3}_{-1.4}$ (see Appendix D in the *Supplemental Material* [11]); the median is close to the power-law exponent used to infer the (higher) merger rates.

VII. ASTROPHYSICAL IMPLICATIONS

GW170104’s source is a heavy stellar-mass binary black hole system. Such binaries are consistent with formation through several different evolutionary pathways [6]. Assuming black holes of stellar origin, there are two broad families of formation channels: dynamical and isolated binary evolution. Dynamical assembly of binaries is expected in dense stellar clusters [84–91]. Dynamical influences are also important for binary coalescences near galactic nuclei [92–94], and through interactions as part of a triple [95, 96]. Isolated binary evolution in galactic fields classically proceeds via a common envelope [97–105]. Variants avoiding common-envelope evolution include (quasi-)chemically homogeneous evolution of massive tidally locked binaries [101, 106, 107], or through stable mass transfer in Population I [108, 109] or Population III binaries [110, 111].

Stars lose mass throughout their lives; to leave a heavy black hole as a remnant they must avoid significant mass loss. Low-metallicity progenitors are believed to have weaker stellar winds and hence diminished mass loss [112]. Given the mass of the primary black hole, the progenitors of GW170104 likely formed in a lower metallicity environment $Z \lesssim 0.5Z_{\odot}$ [6, 100, 113–115], but low mass loss may also have been possible at higher metallicity if the stars were strongly magnetized [116].

An alternative to the stellar-evolution channels would be binaries of primordial black holes [117–120]. GW170104’s component masses lie in a range for which primordial black holes could contribute significantly to

the dark matter content of the Universe, but merger rates in such scenarios are uncertain [118, 121]. The potential for existing electromagnetic observations to exclude primordial black holes of these masses is an active area of research [119, 122–128].

Some of the formation models listed above predict merger rates on the order of $\sim 1\text{--}10 \text{ Gpc}^{-3} \text{ yr}^{-1}$ [85, 87, 92–96, 107, 110, 115]. Given that the rate intervals have now tightened and the lower bound (from the uniform-in-log distribution) is $\sim 12 \text{ Gpc}^{-3} \text{ yr}^{-1}$, these channels may be insufficient to explain the full rate, but they could contribute to the total rate if there are multiple channels in operation. Future observations will improve the precision of the rate estimation, its redshift dependence, and our knowledge of the mass distribution, making it easier to constrain binary formation channels.

Gravitational-wave observations provide information about the component spins through measurements of χ_{eff} , and these measurements can potentially be used to distinguish different formation channels. Dynamically assembled binaries (of both stellar and primordial black holes) should have an isotropic distribution of spin tilts, with equal probability for positive and negative χ_{eff} , and a concentration around zero [129]. Isolated binary evolution typically predicts moderate ($\lesssim 45^\circ$) spin misalignments [130], since the effect of many astrophysical processes, such as mass transfer [131, 132] and tides [133, 134], is to align spins with the orbital angular momentum. Black hole spins could become misaligned due to supernova explosions or torques during collapse. Large natal kicks are needed to produce negative χ_{eff} by changing the orbital plane [129, 130, 135]. The magnitude of these kicks is currently uncertain [136–141] and also influences the merger rate, with high kicks producing lower merger rates in some population-synthesis models [98, 100, 115, 142]. For binary neutron stars there is evidence that large tilts may be possible with small kicks [143–146], and it is not yet understood if similar torques could occur for black holes [138, 147–149]. The absolute value of χ_{eff} depends on the spin magnitudes. Small values of $|\chi_{\text{eff}}|$ can arise because the spin magnitudes are low, or because they are misaligned with the orbital angular momentum or each other. The spin magnitudes for binary black holes are currently uncertain, but GW151226 demonstrated that they can be $\gtrsim 0.2$ [3], and high-mass x-ray binary measurements indicate that the distribution of black hole spins could extend to larger magnitudes [147]. For GW170104, we infer $\chi_{\text{eff}} = -0.12^{+0.21}_{-0.30}$. This includes the possibility of negative χ_{eff} , which would indicate spin-orbit misalignment of at least one component. It also excludes large positive values, and thus could argue against its source forming through chemically homogeneous evolution, since large aligned spins ($a_i \gtrsim 0.4$) would be expected assuming the complete collapse of the progenitor stars [106]. The inferred range is consistent with dynamical assembly and isolated binary evolution provided that the positive orbit-aligned spin is small (whether due to low spins or mis-

alignment) [129, 150–152]. Current gravitational-wave measurements cluster around $\chi_{\text{eff}} \sim 0$ ($|\chi_{\text{eff}}| < 0.35$ at the 90% credible level for all events; see Fig. 10 in the *Supplemental Material* [11]) [5]. Assuming that binary black hole spins are not typically small ($\lesssim 0.2$), our observations hint towards the astrophysical population favoring a distribution of misaligned spins rather than near orbit-aligned spins [153]; further detections will test if this is the case, and enable us to distinguish different spin magnitude and orientation distributions [154–159].

VIII. TESTS OF GENERAL RELATIVITY

To check the consistency of the observed signals with the predictions of GR for binary black holes in quasi-circular orbit, we employ a phenomenological approach that probes how gravitational-wave generation or propagation could be modified in an alternative theory of gravity. Testing for these characteristic modifications in the waveform can quantify the degree to which departures from GR can be tolerated given the data. First, we consider the possibility of a modified gravitational-wave dispersion relation, and place bounds on the magnitude of potential deviations from GR. Second, we perform null tests to quantify generic deviations from GR: without assuming a specific alternative theory of gravity, we verify if the detected signal is compatible with GR. For these tests we use the three confident detections (GW150914, GW151226 and GW170104); we do not use the marginal event LVT151012, as its low SNR means that it contributes insignificantly to all the tests [5].

A. Modified dispersion

In GR, gravitational waves are nondispersive. We consider a modified dispersion relation of the form $E^2 = p^2 c^2 + A p^\alpha c^\alpha$, $\alpha \geq 0$, that leads to dephasing of the waves relative to the phase evolution in GR. Here E and p are the energy and momentum of gravitational radiation, and A is the amplitude of the dispersion [160, 161]. Modifications to the dispersion relation can arise in theories that include violations of local Lorentz invariance [162]. Lorentz invariance is a cornerstone of modern physics but its violation is expected in certain quantum gravity frameworks [162, 163]. Several modified theories of gravity predict specific values of α , including massive-graviton theories ($\alpha = 0$, $A > 0$) [163], multifractal spacetime [164] ($\alpha = 2.5$), doubly special relativity [165] ($\alpha = 3$), and Hořava–Lifshitz [166] and extra-dimensional [167] theories ($\alpha = 4$). For our analysis, we assume that the only effect of these alternative theories is to modify the dispersion relation.

To leading order in $A E^{\alpha-2}$, the group velocity of gravitational waves is modified as $v_g/c = 1 + (\alpha - 1)AE^{\alpha-2}/2$ [161]; both superluminal and subluminal propagation velocities are possible, depending on the sign

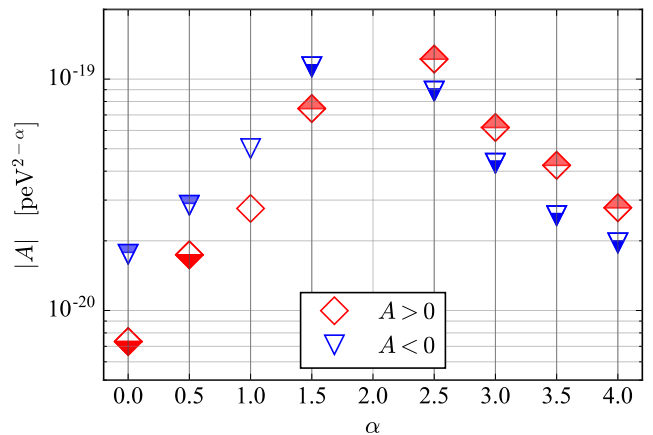


FIG. 5. 90% credible upper bounds on $|A|$, the magnitude of dispersion, obtained combining the posteriors of GW170104 with those of GW150914 and GW151226. We use picoelectronvolts as a convenient unit because the corresponding frequency scale is around where GW170104 has greatest amplitude ($1 \text{ peV} \simeq h \times 250 \text{ Hz}$, where h is the Planck constant). General relativity corresponds to $A = 0$. Markers filled at the top (bottom) correspond to values of $|A|$ and α for which gravitational waves travel with superluminal (subluminal) speed.

of A and the value of α . A change in the dispersion relation leads to an extra term $\delta\Psi(A, \alpha)$ in the evolution of the gravitational-wave phase [160]. We introduce such a term in the effective-precession waveform model [38] to constrain dispersion for various values of α . To this end, we assume flat priors on A . In Fig. 5 we show 90% credible upper bounds on $|A|$ derived from the three confident detections. We do not show results for $\alpha = 2$ since in this case the modification of the gravitational-wave phase is degenerate with the arrival time of the signal.

There exist constraints on Lorentz invariance violating dispersion relations from other observational sectors (e.g., photon or neutrino observations) for certain values of α , and our results are weaker by several orders of magnitude. However, there are frameworks in which Lorentz invariance is only broken in one sector [168, 169], implying that each sector provides complementary information on potential modifications to GR. Our results are the first bounds derived from gravitational-wave observations, and the first tests of superluminal propagation in the gravitational sector.

The result for $A > 0$ and $\alpha = 0$ can be reparametrized to derive a lower bound on the graviton Compton wavelength λ_g , assuming that gravitons disperse in vacuum in the same way as massive particles [5, 7, 170]. In this case, no violation of Lorentz invariance is assumed. Using a flat prior for the graviton mass, we obtain $\lambda_g > 1.5 \times 10^{13} \text{ km}$, which improves on the bound of $1.0 \times 10^{13} \text{ km}$ from previous gravitational-wave observations [5, 7]. The combined bound using the three confident detections is $\lambda_g > 1.6 \times 10^{13} \text{ km}$, or for the graviton mass $m_g \leq 7.7 \times 10^{-23} \text{ eV}/c^2$.

B. Null tests

In the post-Newtonian approximation, the gravitational-wave phase in the Fourier domain is a series expansion in powers of frequency, the expansion coefficients being functions of the source parameters [60, 63, 171]. In the effective-precession model, waveforms from numerical-relativity simulations are also modeled using an expansion of the phase in terms of the Fourier frequency. To verify if the detected signal is consistent with GR, we allow the expansion coefficients to deviate in turn from their nominal GR value and we obtain a posterior distribution for the difference between the measured and GR values [172–177]. We find no significant deviation from the predictions of GR [5, 7]. Combined bounds for GW170104 and the two confident detections from the first observing run [5] do not significantly improve the bounds on the waveform phase coefficients.

Finally, we investigate whether the merger-ringdown portion of the detected signal is consistent with the inspiral part [7, 178, 179]. The two parts are divided at 143 Hz, a frequency close to the median inferred (detector-frame) innermost-stable-circular-orbit frequency of the remnant Kerr black hole. For each part, we infer the component masses and spins, and calculate from these the final mass and spin using fits from numerical relativity, as in Sec. IV [45–48]. We then calculate a two-dimensional posterior distribution for the fractional difference between final mass and spin calculated separately from the two parts [7, 179]. The expected GR value (no difference in the final mass and spin estimates) lies close to the peak of the posterior distribution, well within the 90% credible region. When combined with the posteriors from GW150914, the width of the credible intervals decreases by a factor of ~ 1.5 , providing a better constraint on potential deviations from GR.

In conclusion, in agreement with the predictions of GR, none of the tests we performed indicate a statistically significant departure from the coalescence of Kerr black holes in a quasicircular orbit.

IX. CONCLUSIONS

Advanced LIGO began its second observing run on November 30, 2016, and on January 4, 2017 the LIGO-Hanford and LIGO-Livingston detectors registered a highly significant gravitational-wave signal GW170104 from the coalescence of two stellar-mass black holes. GW170104 joins two other high-significance events [2, 3] and a marginal candidate [4] from Advanced LIGO’s first observing run [5]. This new detection is entirely consistent with the astrophysical rates inferred from the previous run. The source is a heavy binary black hole system, similar to that of GW150914. Spin configurations with both component spins aligned with the orbital angular momentum are disfavored (but not excluded); we do not

significantly constrain the component black holes’ spin magnitudes. The observing run will continue until mid 2017. Expanding the catalog of binary black holes will provide further insight into their formation and evolution, and allow for tighter constraints on potential modifications to GR.

Further details of the analysis and the results are given in the *Supplemental Material* [11]. Data for this event are available at the LIGO Open Science Center [180].

ACKNOWLEDGMENTS

The authors gratefully acknowledge the support of the United States National Science Foundation (NSF) for the construction and operation of the LIGO Laboratory and Advanced LIGO as well as the Science and Technology Facilities Council (STFC) of the United Kingdom, the Max-Planck-Society (MPS), and the State of Niedersachsen/Germany for support of the construction of Advanced LIGO and construction and operation of the GEO 600 detector. Additional support for Advanced LIGO was provided by the Australian Research Council. The authors gratefully acknowledge the Italian Istituto Nazionale di Fisica Nucleare (INFN), the French Centre National de la Recherche Scientifique (CNRS) and the Foundation for Fundamental Research on Matter supported by the Netherlands Organisation for Scientific Research, for the construction and operation of the Virgo detector and the creation and support of the EGO consortium. The authors also gratefully acknowledge research support from these agencies as well as by the Council of Scientific and Industrial Research of India, Department of Science and Technology, India, Science & Engineering Research Board (SERB), India, Ministry of Human Resource Development, India, the Spanish Ministerio de Economía y Competitividad, the Vicepresidència i Conselleria d’Innovació, Recerca i Turisme and the Conselleria d’Educació i Universitat del Govern de les Illes Balears, the National Science Centre of Poland, the European Commission, the Royal Society, the Scottish Funding Council, the Scottish Universities Physics Alliance, the Hungarian Scientific Research Fund (OTKA), the Lyon Institute of Origins (LIO), the National Research Foundation of Korea, Industry Canada and the Province of Ontario through the Ministry of Economic Development and Innovation, the Natural Science and Engineering Research Council Canada, Canadian Institute for Advanced Research, the Brazilian Ministry of Science, Technology, and Innovation, International Center for Theoretical Physics South American Institute for Fundamental Research (ICTP-SAIFR), Russian Foundation for Basic Research, the Leverhulme Trust, the Research Corporation, Ministry of Science and Technology (MOST), Taiwan and the Kavli Foundation. The authors gratefully acknowledge the support of the NSF, STFC, MPS, INFN, CNRS and the State of Niedersachsen/Germany for provision of computational resources. This article has been

assigned the document number LIGO-P170104.

SUPPLEMENTAL MATERIAL

Appendix A: Noise performance of the detectors

Figure 6 shows a comparison of typical strain noise amplitude spectra during the first observing run and early in the second for both of the LIGO detectors [181]. For the Hanford detector, shot-noise limited performance was improved above about 500 Hz by increasing the laser power. There are new broad mechanical resonance features (e.g., at ~ 150 Hz, 320 Hz and 350 Hz) due to increased beam pointing jitter from the laser, as well as the coupling of the jitter to the detector’s gravitational-wave channel that is larger than in the Livingston detector. The increase in the noise between 40 Hz and 100 Hz is currently under investigation. For the Livingston detector, significant reduction in the noise between 25 Hz and 100 Hz was achieved mainly by the reduction of the scattered light that re-enters the interferometer.

To date, the network duty factor of the LIGO detectors in the second observing run is about 51% while it was about 43% in the first observing run. The improvement came from better seismic isolation at Hanford, and fine tuning of the control of the optics at Livingston.

Appendix B: Searches

The significance of a candidate event is calculated by comparing its detection statistic value to an estimate of the background noise [4, 16, 17, 22, 31]. Figure 7 shows the background and candidate events from the offline searches for compact binary coalescences obtained from 5.5 days of coincident data. At the detection statistic value assigned to GW170104, the false alarm rate is less than 1 in 70,000 years of coincident observing time.

Appendix C: Parameter inference

The source properties are estimated by exploring the parameter space with stochastic sampling algorithms [36]. Calculating the posterior probability requires the likelihood of the data given a set of parameters, and the parameters’ prior probabilities. The likelihood is determined from a noise-weighted inner product between the data and a template waveform [59]. Possible calibration error is incorporated using a frequency-dependent spline model for each detector [183]. The analysis follows the approach used for previous signals [5, 37, 44].

A preliminary analysis was performed to provide a medium-latency source localization [184]. This analysis used an initial calibration of the data and assumed a (conservative) one-sigma calibration uncertainty of 10% in amplitude and 10° in phase for both detectors, a reduced-order quadrature model of the effective-precession waveform [38, 40, 185, 186] (the most computationally expedient model), and a power spectral den-

sity calculated using a parametrized model of the detector noise [82, 187]. A stretch of 4 s of data, centered on the event, was analysed across a frequency range of 20–1024 Hz. We assumed uninformative prior probabilities [5, 37]; technical restrictions of the reduced-order quadrature required us to limit spin magnitudes to < 0.8 and impose cuts on the masses (as measured in the detector frame) such that $m_{1,2}^{\text{det}} \in [5.5, 160] M_{\odot}$, $\mathcal{M}^{\text{det}} \in [12.3, 45.0] M_{\odot}$ and mass ratio $q = m_2/m_1 \geq 1/8$. The bounds of the mass prior do not affect the posterior, but the spin distributions were truncated. The source position is not strongly coupled to the spin distribution, and so should not have been biased by these limits [18, 77].

The final analysis used an updated calibration of the data, with one-sigma uncertainties of 3.8% in amplitude and 2.2° in phase for Hanford, and 3.8% and 1.9° for Livingston, and two waveform models, the effective-precession model [38, 40, 186] and the full-precession model [41–43]. The spin priors were extended up to 0.99. As a consequence of the computational cost of the full-precession model, we approximate the likelihood by marginalising over the time and phase at coalescence as if the waveform contained only the dominant $(2, \pm 2)$ harmonics [36]. This marginalisation is not exact for precessing models, but should not significantly affect signals with binary inclinations that are nearly face on or face off [44]. Comparisons with preliminary results from an investigation using the full-precession waveform without marginalisation confirm that this approximation does not impact results. The two waveform models produce broadly consistent parameter estimates, so the overall results are constructed by averaging the two distributions. As a proxy for the theoretical error from waveform modeling, we use the difference between the results from the two approximants [37]. A detailed summary of results is given in Table II, and the final sky localization is shown in Fig. 8.

Figure 9 illustrates the distance, and the angle between the total angular momentum and the line of sight θ_{JN} . The latter is approximately constant throughout the inspiral and serves as a proxy for the binary inclination [62, 188]. The full-precessing model shows a greater preference (after accounting for the prior) for face-on or face-off orientations with $\theta_{JN} \simeq 0^\circ$ or 180° . This leads to the tail of the D_L distribution extending to farther distances. There is a preference towards face-on or face-off inclinations over those which are edge on; the probability that $|\cos \theta_{JN}| > 1/\sqrt{2}$ is 0.62, compared to a prior probability of 0.29. These inclinations produce louder signals and so are expected to be most commonly detected [189, 190]. Viewing the binary near face-on or face-off minimises the impact (if present) of precession [37, 61].

For GW170104, we obtain weak constraints on the spins. The amount of information we learn from the signal may be quantified by the Kullback–Leibler divergence, or relative entropy, from the prior to the posterior [191, 192]. For χ_{eff} we gain 0.36 nat of information, and for χ_p we only gain 0.03 nat. As compari-

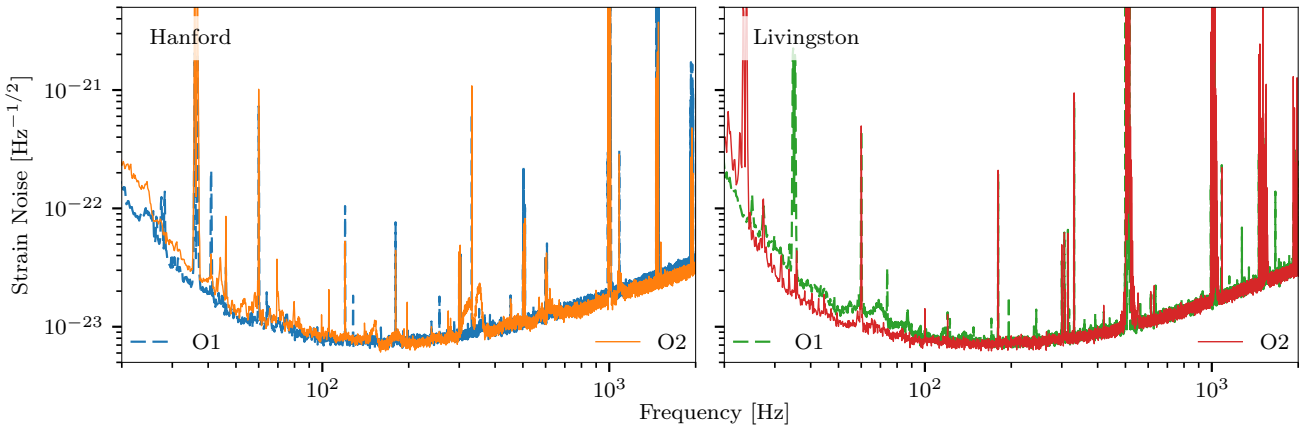


FIG. 6. Comparison of typical noise amplitude spectra of the LIGO detectors in the first observing run (O1) and the early stages of the second observing run (O2). The noise is expressed in terms of equivalent gravitational-wave strain amplitude. Some narrow features are calibration lines (22–24 Hz for L1, 35–38 Hz for H1, 330 Hz and 1080 Hz for both), suspension fibers’ resonances (500 Hz and harmonics) and 60 Hz power line harmonics.

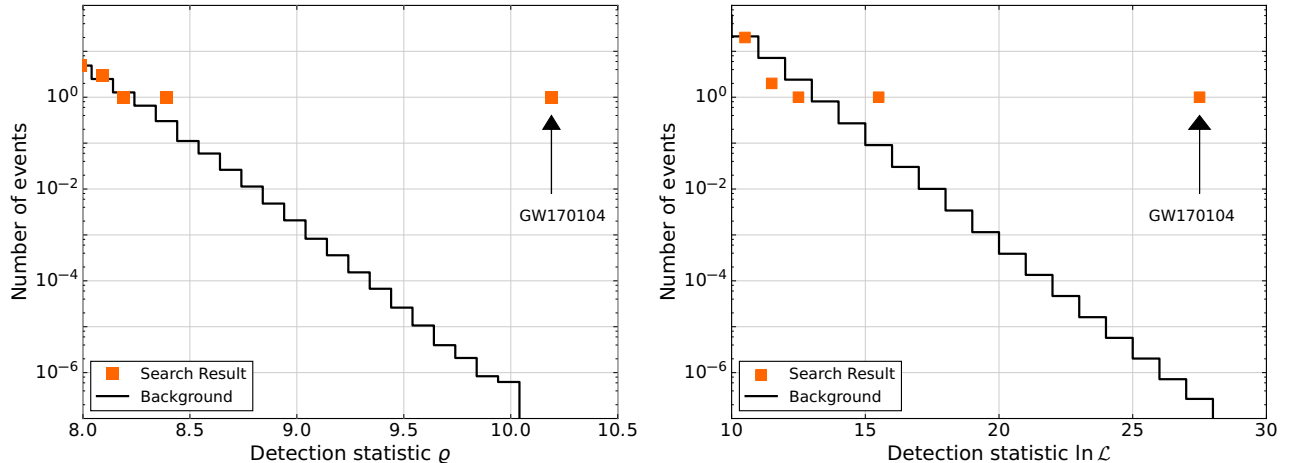


FIG. 7. *Left:* Search results from the binary coalescence search described in [16, 17, 31]. The histogram shows the number of candidate events (orange markers) in the 5.5 days of coincident data and the expected background (black lines) as a function of the search detection statistic. The reweighted SNR detection statistic ϱ is defined in [31]. GW170104 has a larger detection statistic value than all of the background events in this period. At the detection statistic value assigned to GW170104, the search’s false alarm rate is less than 1 in 70,000 years of coincident observing time. No other significant candidate events are observed in this time interval. *Right:* Search results from an independently-implemented analysis [22], where the detection statistic $\ln \mathcal{L}$ is an approximate log likelihood ratio statistic that is an extension of [182]. The two search algorithms give consistent results.

son, the Kullback–Leibler divergence between two equal-width normal distributions with means one standard deviation apart is $0.5 \text{ nat} = 0.72 \text{ bit}$. We cannot gain much insight from these spin measurements, but this may become possible by considering the population of binary black holes [193]. Figure 10 shows the inferred χ_{eff} distributions for GW170104, GW150914, LVT151012 and GW151226 [5]. Only GW151226 has a χ_{eff} (and hence at least one component spin) inconsistent with zero. The others are consistent with positive or negative effective inspiral spin parameters; the probabilities that $\chi_{\text{eff}} > 0$ are 0.18, 0.23 and 0.59 for GW170104, GW150914 and LVT151012, respectively. Future analy-

sis may reveal if there is evidence for spins being isotropically distributed, preferentially aligned with the orbital angular momentum, or drawn from a mixture of populations [153, 155, 158, 159].

While we learn little about the component spin magnitudes, we can constrain the final black hole spin. The final black hole’s dimensionless spin a_f is set by the binary’s total angular momentum (the orbital angular momentum and the components’ spins) minus that radiated away. Figure 11 illustrates the probability distributions for the final mass and spin. To obtain these, we average results from different numerical-relativity calibrated fits for the final mass [46, 47] and for the final

TABLE II. Parameters describing GW170104. We report the median value with symmetric (equal-tailed) 90% credible interval, and selected 90% credible bounds. Results are given for effective- and full-precession waveform models; the overall results average the posteriors for the two models. The overall results include a proxy for the 90% range of systematic error estimated from the variance between models. More details of the parameters, and the imprint they leave on the signal, are explained in [37]. The optimal SNR is the noise-weighted inner product of the waveform template with itself, whereas the matched-filter SNR is the inner product of the template with the data.

| | Effective precession | Full precession | Overall |
|---|---------------------------|---------------------------|---|
| Detector-frame | | | |
| Total mass M^{det}/M_{\odot} | $60.0^{+5.7}_{-5.8}$ | $59.9^{+5.7}_{-6.9}$ | $59.9^{+5.7 \pm 0.1}_{-6.5 \pm 1.0}$ |
| Chirp mass $\mathcal{M}^{\text{det}}/M_{\odot}$ | $24.9^{+2.5}_{-3.5}$ | $25.2^{+2.4}_{-4.2}$ | $25.1^{+2.5 \pm 0.2}_{-3.9 \pm 0.4}$ |
| Primary mass $m_1^{\text{det}}/M_{\odot}$ | $37.1^{+9.2}_{-7.0}$ | $36.3^{+8.7}_{-6.5}$ | $36.7^{+9.0 \pm 1.2}_{-6.8 \pm 0.4}$ |
| Secondary mass $m_2^{\text{det}}/M_{\odot}$ | $22.6^{+6.5}_{-7.2}$ | $23.3^{+5.9}_{-7.8}$ | $22.9^{+6.2 \pm 0.2}_{-7.5 \pm 0.1}$ |
| Final mass $M_f^{\text{det}}/M_{\odot}$ | $57.6^{+5.6}_{-5.3}$ | $57.4^{+5.4}_{-6.1}$ | $57.5^{+5.5 \pm 0.3}_{-5.8 \pm 0.8}$ |
| Source-frame | | | |
| Total mass M/M_{\odot} | $51.0^{+5.8}_{-4.9}$ | $50.4^{+5.9}_{-5.1}$ | $50.7^{+5.9 \pm 0.5}_{-5.0 \pm 0.6}$ |
| Chirp mass \mathcal{M}/M_{\odot} | $21.1^{+2.4}_{-2.5}$ | $21.1^{+2.3}_{-2.8}$ | $21.1^{+2.4 \pm 0.1}_{-2.7 \pm 0.3}$ |
| Primary mass m_1/M_{\odot} | $31.6^{+8.8}_{-6.3}$ | $30.7^{+8.1}_{-5.9}$ | $31.2^{+8.4 \pm 1.3}_{-6.0 \pm 0.4}$ |
| Secondary mass m_2/M_{\odot} | $19.2^{+5.4}_{-5.7}$ | $19.6^{+5.0}_{-6.2}$ | $19.4^{+5.3 \pm 0.1}_{-5.9 \pm 0.0}$ |
| Final mass M_f/M_{\odot} | $49.0^{+5.7}_{-4.6}$ | $48.4^{+5.7}_{-4.7}$ | $48.7^{+5.7 \pm 0.6}_{-4.6 \pm 0.6}$ |
| Energy radiated $E_{\text{rad}}/(M_{\odot}c^2)$ | $2.0^{+0.6}_{-0.7}$ | $2.1^{+0.5}_{-0.8}$ | $2.0^{+0.6 \pm 0.0}_{-0.7 \pm 0.0}$ |
| Mass ratio q | $0.60^{+0.33}_{-0.26}$ | $0.64^{+0.31}_{-0.27}$ | $0.62^{+0.32 \pm 0.01}_{-0.26 \pm 0.02}$ |
| Effective inspiral spin parameter χ_{eff} | $-0.12^{+0.20}_{-0.26}$ | $-0.11^{+0.21}_{-0.33}$ | $-0.12^{+0.21 \pm 0.01}_{-0.30 \pm 0.05}$ |
| Effective precession spin parameter χ_p | $0.42^{+0.41}_{-0.29}$ | $0.40^{+0.42}_{-0.30}$ | $0.41^{+0.41 \pm 0.00}_{-0.30 \pm 0.02}$ |
| Dimensionless primary spin magnitude a_1 | $0.45^{+0.44}_{-0.40}$ | $0.44^{+0.48}_{-0.40}$ | $0.45^{+0.46 \pm 0.02}_{-0.40 \pm 0.01}$ |
| Dimensionless secondary spin magnitude a_2 | $0.50^{+0.44}_{-0.45}$ | $0.44^{+0.48}_{-0.40}$ | $0.47^{+0.46 \pm 0.01}_{-0.43 \pm 0.01}$ |
| Final spin a_f | $0.63^{+0.10}_{-0.19}$ | $0.64^{+0.09}_{-0.20}$ | $0.64^{+0.09 \pm 0.01}_{-0.20 \pm 0.00}$ |
| Luminosity distance D_L/Mpc | 860^{+410}_{-370} | 910^{+470}_{-410} | $880^{+450 \pm 90}_{-390 \pm 10}$ |
| Source redshift z | $0.173^{+0.072}_{-0.071}$ | $0.182^{+0.081}_{-0.078}$ | $0.176^{+0.078 \pm 0.015}_{-0.074 \pm 0.001}$ |
| Upper bound | | | |
| Effective inspiral spin parameter χ_{eff} | 0.04 | 0.05 | 0.04 ± 0.01 |
| Effective precession spin parameter χ_p | 0.74 | 0.74 | 0.74 ± 0.01 |
| Primary spin magnitude a_1 | 0.82 | 0.86 | 0.84 ± 0.03 |
| Secondary spin magnitude a_2 | 0.89 | 0.86 | 0.88 ± 0.02 |
| Lower bound | | | |
| Mass ratio q | 0.40 | 0.42 | 0.41 ± 0.02 |
| Optimal SNR $\rho_{(h h)}$ | $13.0^{+1.7}_{-1.7}$ | $12.9^{+1.7}_{-1.7}$ | $13.0^{+1.7 \pm 0.0}_{-1.7 \pm 0.0}$ |
| Matched-filter SNR $\rho_{(h s)}$ | $13.3^{+0.2}_{-0.3}$ | $13.3^{+0.2}_{-0.3}$ | $13.3^{+0.2 \pm 0.0}_{-0.3 \pm 0.0}$ |

spin [45–47]. The fitting formulae take the component masses and spins as inputs. We evolve the spins forward from the 20 Hz reference frequency to a fiducial near merger frequency, and augment the aligned-spin final spin fits [46, 47] with the contribution from the in-plane spins before averaging [48]. From comparisons with precessing numerical-relativity results, we estimate that systematic errors are negligible compared to the statistical uncertainties. We follow the same approach for fits for the peak luminosity [47, 49]; here the systematic errors are larger (up to $\sim 10\%$) and we include them in the uncertainty estimate [37]. We find that $a_f = 0.64^{+0.09}_{-0.20}$. This is comparable to that for previous events [5, 37, 44],

as expected for near equal-mass binaries [194, 195], but extends to lower values because of the greater preference for spins with components antialigned with the orbital angular momentum.

The final calibration uncertainty is sufficiently small to not significantly affect results. To check the impact of calibration uncertainty, we repeated the analysis using the effective-precession waveform without marginalising over the calibration. For most parameters the change is negligible. The most significant effect of calibration uncertainty is on sky localization. Excluding calibration uncertainty reduces the 90% credible area by $\sim 2\%$.

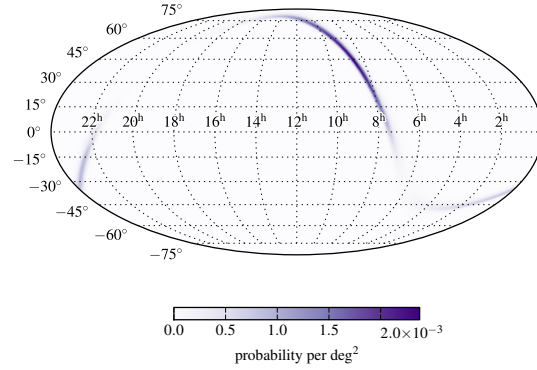


FIG. 8. A Mollweide projection of the posterior probability density for the location of the source in equatorial coordinates (right ascension is measured in hours and declination is measured in degrees). The location broadly follows an annulus corresponding to a time delay of $\sim 3.0^{+0.4}_{-0.5}$ ms between the Hanford and Livingston observatories. We estimate that the area of the 90% credible region is $\sim 1200 \text{ deg}^2$.

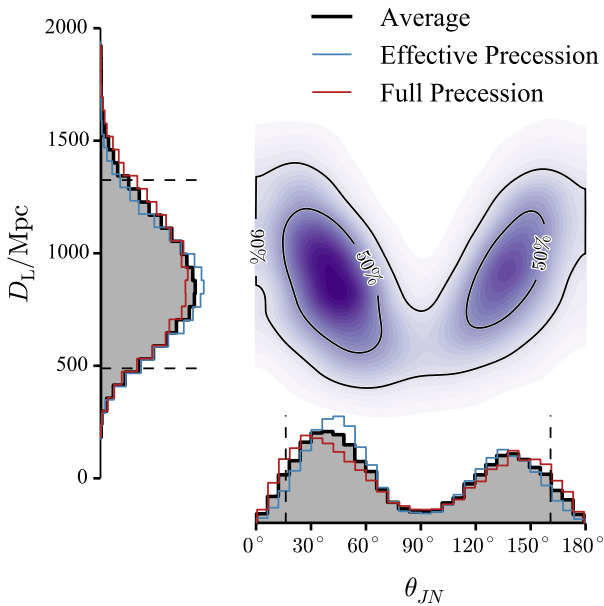


FIG. 9. Posterior probability density for the source luminosity distance D_L and the binary inclination θ_{JN} . The one-dimensional distributions include the posteriors for the two waveform models, and their average (black). The dashed lines mark the 90% credible interval for the average posterior. The two-dimensional plot shows the 50% and 90% credible regions plotted over the posterior density function.

Appendix D: Population inference

Gravitational-wave observations are beginning to reveal a population of merging binary black holes. With four probable mergers we can only roughly constrain the population. Here we fit a hierarchical single-parameter

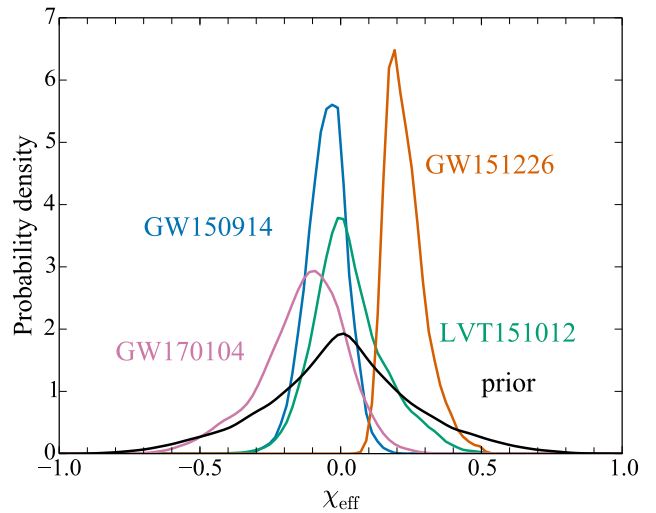


FIG. 10. Posterior probability densities for the effective inspiral spin χ_{eff} for GW170104, GW150914, LVT151012 and GW151226 [5], together with the prior probability distribution for GW170104. The distribution for GW170104 uses both precessing waveform models, but, for ease of comparison, the others use only the effective-precession model. The prior distributions vary between events, as a consequence of different mass ranges, but the difference is negligible on the scale plotted.

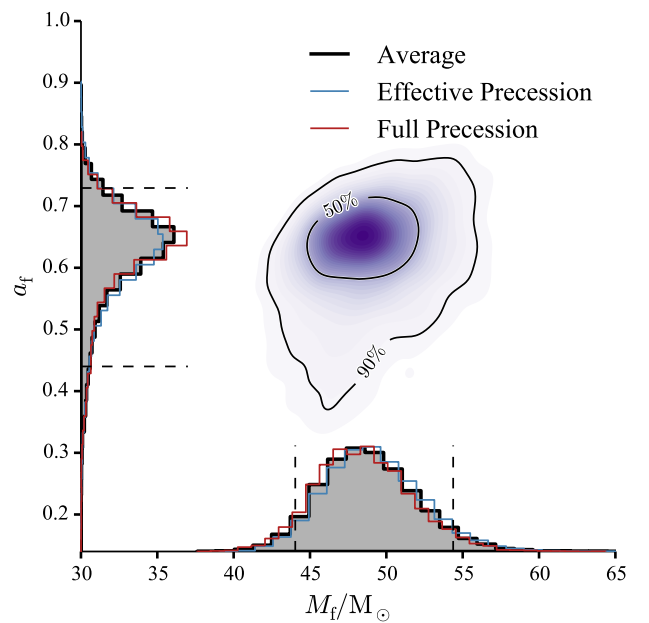


FIG. 11. Posterior probability density for the final black hole mass M_f and spin magnitude a_f . The one-dimensional distributions include the posteriors for the two waveform models, and their average (black). The dashed lines mark the 90% credible interval for the average posterior. The two-dimensional plot shows the 50% and 90% credible regions plotted over the posterior density function.

population model to the three probable mergers from first observing run [5] and GW170104. We assume that the two-dimensional mass distribution of mergers is the combination of a power law in m_1 and a flat m_2 distribution,

$$p(m_1, m_2) \propto m_1^{-\alpha} \frac{1}{m_1 - m_{\min}}, \quad (\text{D1})$$

with $m_{\min} = 5 M_\odot$ [196–198], and subject to the constraint that $M \leq M_{\max}$, with $M_{\max} = 100 M_\odot$, matching the analysis from the first observing run [5, 8]. Our sensitivity to these choices for lower and upper cut-off masses is much smaller than the statistical uncertainty in our final estimate of α . The marginal distribution for m_1 is

$$p(m_1) \propto m_1^{-\alpha} \frac{\min(m_1, M_{\max} - m_1) - m_{\min}}{m_1 - m_{\min}}, \quad (\text{D2})$$

and the parameter α is the power-law slope of the marginal distribution for m_1 at masses $m_1 \leq M_{\max}/2$. The initial mass function of stars follows a similar power-law distribution [83, 199], and the mass distribution of companions to massive stars appears to be approximately uniform in the mass ratio q [200–202]. While the initial-final mass relation in binary black hole systems is complicated and nonlinear [114, 203–205], this simple form provides a sensible starting point for estimating the mass distribution.

Accounting for selection effects and the uncertainty in our estimates of the masses of our four events, and imposing a flat prior on the parameter α [5], we find $\alpha = 2.3^{+1.3}_{-1.4}$. Our posterior on α appears in Fig. 12. The inferred posterior on the marginal distribution for m_1 appears in Fig. 13; the turnover for $m_1 > 50 M_\odot$ is a consequence of our choice of $M_{\max} = 100 M_\odot$ in Eq. (D2).

Appendix E: Tests of general relativity

The tests of GR use the same algorithm base described in Sec. C [36] for estimation of source parameters, with appropriate modifications to the analytical waveform models [5, 7]. In the Fourier domain, gravitational waves from a coalescing binary can be described by

$$\tilde{h}_{\text{GR}}(f) = \tilde{A}(f; \vec{\vartheta}_{\text{GR}}) e^{i\Psi(f; \vec{\vartheta}_{\text{GR}})}, \quad (\text{E1})$$

where $\vec{\vartheta}_{\text{GR}}$ are the parameters of the source (e.g., masses and spins) in GR. The tests of GR we perform, except for the inspiral–merger–ringdown consistency test, introduce a dephasing term with an unknown prefactor that captures the magnitude of the deviation from GR. While we modify the phase of the waveform from its GR value, the amplitude is kept unchanged; this is because our analysis is more sensitive to the phase evolution than the amplitude. We use a non-GR template of the form

$$\tilde{h}(f) = \tilde{A}(f; \vec{\vartheta}_{\text{GR}}) e^{i[\Psi(f; \vec{\vartheta}_{\text{GR}}) + \delta\Psi(f; \vec{\vartheta}_{\text{GR}}, X_{\text{modGR}})]}, \quad (\text{E2})$$

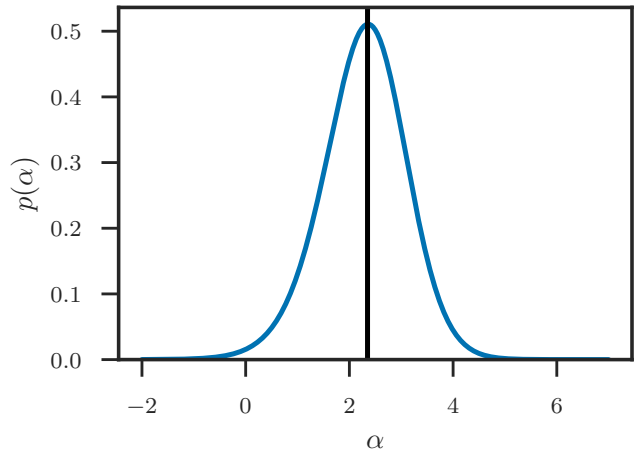


FIG. 12. The posterior distribution for the power-law slope of the massive component of the binary black hole mass distribution, α , described in the main text, using the three probable events from the first observing run [5] and GW170104. We find the median and 90% credible interval are $\alpha = 2.3^{+1.3}_{-1.4}$. The black line indicates the Salpeter law [83] slope used in the power-law population for estimating binary black hole coalescence rates.

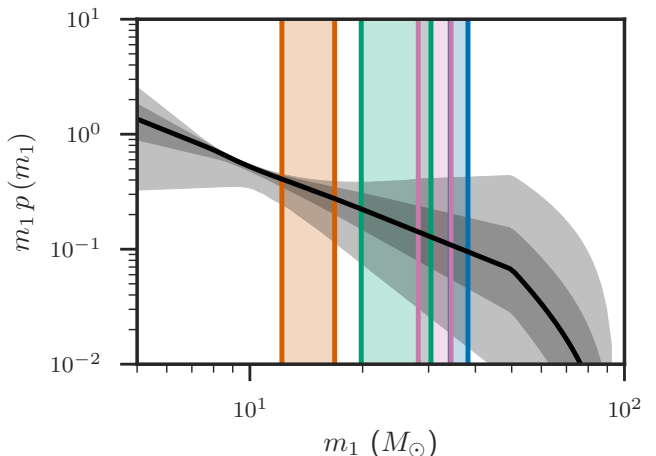


FIG. 13. The posterior probability distribution for the primary component mass m_1 of binary black holes inferred from the hierarchical analysis. The black line gives the posterior median as a function of mass, and the dark and light grey bands give the 50% and 90% credible intervals. The colored vertical bands give the 50% credible interval from the posterior on m_1 from the analyses of (left to right) GW151226, LVT151012, GW170104, and GW150914. The marginal mass distribution is a power law for $m_1 \leq 50 M_\odot$, and turns over for $m_1 \geq 50 M_\odot$ due to the constraint on the two-dimensional population distribution that $m_1 + m_2 \leq 100 M_\odot$.

where X_{modGR} is a theory-dependent parameter, which is zero in the usual GR templates. To simulate the non-GR waveform, we used the effective-precession model as a base; all the GR and non-GR parameters are assumed unknown and estimated from the data.

With multiple detections it is possible to combine constraints on X_{modGR} to obtain tighter bounds. For a generic parameter ϑ , we compute a combined posterior distribution by combining the individual likelihoods [206]. For each event e_i we estimate the marginal likelihood density $p(e_i|\vartheta)$ using a Gaussian kernel density estimator. This gives a simple representation of the likelihood that can be easily manipulated. The combined posterior distribution is computed by multiplying the marginal likelihoods and the chosen prior distribution,

$$p(\vartheta|e_1, \dots, e_N) \propto p(\vartheta) \prod_{i=1}^N p(e_i|\vartheta). \quad (\text{E3})$$

This is used to compute bounds on ϑ given N detections. We use the three confident detections (GW150914, GW151226 and GW170104) to set combined bounds on potential deviation from GR, except in the case of the inspiral–merger–ringdown consistency test where only GW150914 and GW170104 are used as GW151226 has insufficient SNR from the merger–ringdown to make useful inferences.

1. Modified dispersion

We have assumed a generic dispersion relation of the form $E^2 = p^2 c^2 + A p^\alpha c^\alpha$, $\alpha \geq 0$. To leading order in $A E^{\alpha-2}$, the group velocity of gravitational waves is thus modified as $v_g/c = 1 + (\alpha - 1) A E^{\alpha-2}/2$. The modified dispersion relation results in an extra term to be added to the gravitational-wave phase [160]:

$$\delta\Psi = \begin{cases} \frac{\pi}{\alpha-1} \frac{AD_\alpha}{(hc)^{2-\alpha}} \left[\frac{(1+z)f}{c} \right]^{\alpha-1} & \alpha \neq 1 \\ \frac{\pi AD_\alpha}{hc} \ln \left(\frac{\pi G \mathcal{M}^{\text{det}} f}{c^3} \right) & \alpha = 1 \end{cases}. \quad (\text{E4})$$

Here \mathcal{M}^{det} is the redshifted (detector-frame) chirp mass, h is the Planck constant, and D_α is a distance measure,

$$D_\alpha = \frac{1+z}{H_0} \int_0^z \frac{(1+z')^{\alpha-2}}{\sqrt{\Omega_m(1+z')^3 + \Omega_\Lambda}} dz', \quad (\text{E5})$$

where H_0 is the Hubble constant, Ω_m and Ω_Λ are the matter and dark energy density parameters [52], respectively.

Table III lists the 90% credible upper bounds on the magnitude of A , where the individual and combined bounds for the three confident detections are shown; we see that depending on the value of α and the sign of A , the combined bounds are better than those obtained from GW170104 alone by a factor of $\sim 1\text{--}4.5$. For all values of α , these bounds are consistent with the uncertainties one might expect for heavy binary black holes using Fisher-matrix estimates on simulated GW150914-like signals [161].

For small values of α , it is useful to recast the results in terms of lower bounds on a length scale $\lambda_A = hcA^{1/(\alpha-2)}$, which can be thought of as the range (or the screening length) of an effective potential, which is infinite in GR. In Table IV we report the numerical values of these bounds for $\alpha < 2$. For $\alpha = 3, 4$, we instead express the bounds as lower limits on the energy scale at which quantum gravity effects might become important, $E_{\text{QG}} = A^{-1/(\alpha-2)}$ [207–211]. This facilitates the comparison with existing constraints from other sectors, which we show in Table V.

In the subluminal propagation regime, bounds exist from electromagnetic (spectral time lag in gamma-ray bursts [210]), neutrino (time delay between neutrino and photons from blazar PKS B1424-418 [211]), and gravitational (absence of gravitational Cherenkov radiation [207, 209]) sectors. In the superluminal propagation regime, the only existing limits are from the neutrino sector (absence of Bremsstrahlung from electron–positron pairs [208]). The GW170104 constraints are weaker than existing bounds, but are the first constraints on Lorentz violation in the gravitational superluminal-propagation sector.

The posterior distributions for A have long tails, which makes it difficult to accurately calculate 90% limits with a finite number of samples. To quantify this uncertainty on the bounds, for each value of α and sign of A we use Bayesian bootstrapping [212] to generate 1000 instances of the relevant posterior distribution. We find that the 90% credible upper bounds are estimated within an interval whose 90% credible interval width is $\lesssim 20\%$ of the values reported in Table III.

For the (GR) source parameters, to check for the potential impact of errors from waveform modelling, we analysed the data using both the effective-precession model and the full-precession model. However, the full-precession model was not adapted in time for tests of GR to be completed for this publication. In the first observing run, we performed tests with two different waveform families [5, 7]: the effective-precession model [38, 40, 186], and a nonprecessing waveform model [42, 213]. We follow the same approach here, and use the same nonprecessing waveform model used for the matched filter search [29]. The use of a nonprecessing waveform should give conservative bounds on the potential error from waveform modelling, as some of the differences may come from the failure to include precession effects [44]. We find that the numbers so obtained are consistent with the results of the effective-precession model at the tens of percent level.

2. Parametrized test

The phase evolution of gravitational waves from compact binaries is well understood within GR. The inspiral portion, corresponding to large orbital separation, can be described analytically using the post-Newtonian

TABLE III. 90% credible level upper bounds on the Lorentz violation magnitude $|A/\text{eV}^{2-\alpha}|$ using GW150914, GW151226, GW170104, and their joint posterior.

| α | $A > 0$ | | | | $A < 0$ | | | |
|----------|-----------------------|-----------------------|-----------------------|-----------------------|-----------------------|-----------------------|-----------------------|-----------------------|
| | GW150914 | GW151226 | GW170104 | Joint | GW150914 | GW151226 | GW170104 | Joint |
| 0.0 | 1.3×10^{-44} | 1.7×10^{-43} | 9.8×10^{-45} | 7.3×10^{-45} | 2.3×10^{-44} | 7.1×10^{-44} | 3.6×10^{-44} | 1.8×10^{-44} |
| 0.5 | 4.8×10^{-38} | 1.6×10^{-37} | 1.8×10^{-38} | 1.7×10^{-38} | 4.1×10^{-38} | 9.4×10^{-38} | 7.8×10^{-38} | 2.9×10^{-38} |
| 1.0 | 8.5×10^{-32} | 1.8×10^{-31} | 3.6×10^{-32} | 2.8×10^{-32} | 1.0×10^{-31} | 1.3×10^{-31} | 1.0×10^{-31} | 5.0×10^{-32} |
| 1.5 | 1.9×10^{-25} | 3.2×10^{-25} | 9.4×10^{-26} | 7.5×10^{-26} | 2.7×10^{-25} | 2.2×10^{-25} | 2.3×10^{-25} | 1.1×10^{-25} |
| 2.5 | 3.9×10^{-13} | 1.4×10^{-13} | 2.8×10^{-13} | 1.2×10^{-13} | 2.8×10^{-13} | 2.0×10^{-13} | 1.3×10^{-13} | 8.9×10^{-14} |
| 3.0 | 2.2×10^{-07} | 7.4×10^{-08} | 1.7×10^{-07} | 6.2×10^{-08} | 1.7×10^{-07} | 1.5×10^{-07} | 8.9×10^{-08} | 4.3×10^{-08} |
| 3.5 | 1.7×10^{-01} | 5.4×10^{-02} | 1.4×10^{-01} | 4.2×10^{-02} | 1.2×10^{-01} | 1.1×10^{-01} | 7.1×10^{-02} | 2.6×10^{-02} |
| 4.0 | $1.3 \times 10^{+05}$ | $5.9 \times 10^{+04}$ | $1.0 \times 10^{+05}$ | $2.8 \times 10^{+04}$ | $9.7 \times 10^{+04}$ | $1.3 \times 10^{+05}$ | $7.7 \times 10^{+04}$ | $2.0 \times 10^{+04}$ |

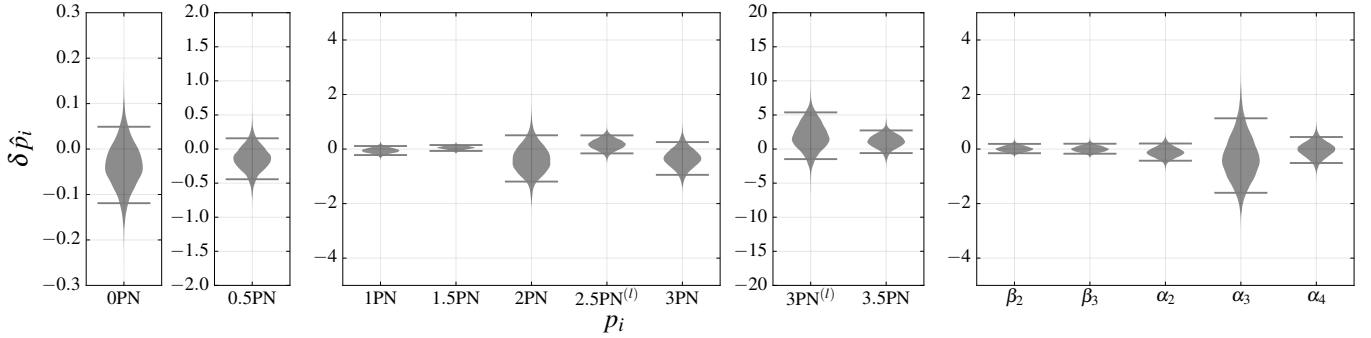


FIG. 14. Violin plots for the parametrized test, combining posteriors for GW170104 with the two confident detections made in the first observing run, GW150914 and GW151226 [5]. This figure has been corrected according to [228], and its 90% bars have been re-positioned to correct a previous plotting error.

TABLE IV. 90% credible level lower bounds on the length scale λ_A for Lorentz invariance violation test using GW170104 alone.

| | $A > 0$ | $A < 0$ |
|----------------|-------------------------|-------------------------|
| $\alpha = 0.0$ | 1.3×10^{13} km | 6.6×10^{12} km |
| $\alpha = 0.5$ | 1.8×10^{16} km | 6.8×10^{15} km |
| $\alpha = 1.0$ | 3.5×10^{22} km | 1.2×10^{22} km |
| $\alpha = 1.5$ | 1.4×10^{41} km | 2.4×10^{40} km |

expansion [63]. Modelling the merger dynamics requires the use of numerical-relativity simulations [214–216], whereas the post-merger signal is described in black hole perturbation theory as a superposition of damped sinusoids [217–220]. Accurate analytical waveforms are obtained by tuning the effective-one-body [29, 221, 222] or phenomenological models [40, 223] to numerical-relativity simulations [186, 224, 225].

Given a phase parameter in the phenomenological model whose value in GR is p_i , we modify the waveform by introducing new dimensionless parameters $\delta\hat{p}_i$ such that $p_i \rightarrow p_i(1 + \delta\hat{p}_i)$ [5, 7]. In the parametrized null test, we freely vary one $\delta\hat{p}_i$ at a time (in addition to

TABLE V. 90% confidence level lower bounds on the energy scale at which quantum gravity effects might become important E_{QG} . Bounds are grouped into theories which produce subluminal and superluminal gravitational-wave propagation. The results from GW170104 are considerably less constraining than those obtained with other methods, but they are the first direct constraints of Lorentz invariance violation in the superluminal gravity sector.

| | | $\alpha = 3$ | $\alpha = 4$ |
|-----|----------------------|-------------------------|-------------------------|
| Sub | GW170104 | 1.1×10^7 eV | 3.6×10^{-3} eV |
| | Gamma rays [210] | 5×10^{24} eV | 1.4×10^{16} eV |
| | Neutrino [211] | 1.2×10^{26} eV | 7.3×10^{20} eV |
| | Cherenkov [207, 209] | 4.6×10^{35} eV | 5.2×10^{27} eV |
| | GW170104 | 6.0×10^6 eV | 3.2×10^{-3} eV |
| | Neutrino [208] | 1.2×10^{33} eV | 1.2×10^{24} eV |

the other source parameters) to look for deviations from GR.

The bounds on \hat{p}_i obtained from GW170104 are weaker than those from the two confident detections of the first observing run [5]. GW151226 had an SNR comparable to GW170104, but it is from a significantly lower

mass system [3, 5], and hence places better constraints on the inspiral parameters. GW150914 had an SNR twice that of GW170104 (while being of comparable mass), and thus places the best constraints on the late-inspiral and merger–ringdown parameters. Therefore, instead of reporting bounds from GW170104, we provide updated combined bounds, combining the results from the three events. In Fig. 14 we show a violin plot for each of the test parameters. The parameters are plotted (from the left) following the order in which they appear in the post-Newtonian expansion or enter the phenomenological model (the β and α parameters). For all the parameters, the GR solution ($\delta\hat{p}_i = 0$) is contained in the 90% credible interval.

3. Inspiral–merger–ringdown consistency test

GR is well tested in weak gravitational fields, but fewer tests have been performed in the strong-field regime [163, 226, 227]. It is possible that deviations from the expected behavior of GR only manifest in the most extreme conditions, where spacetime is highly dynamical. The inspiral–merger–ringdown consistency test checks whether the low-frequency, inspiral-dominated portion of the waveform is consistent with the high-frequency, merger–ringdown portion. The two frequency ranges

are analysed separately, and the inferred parameters are compared. The test uses the estimated final black hole mass and spin (calculated from the component masses and spins using numerical-relativity fits as detailed in Sec. C) [7, 178]. If the waveform is compatible with the predictions of GR, we expect that the parameters inferred from the two pieces will be consistent with each other, although the difference will not, in general, be zero because of detector noise. In Fig. 15, we show the posteriors on the fractional difference in the two estimates of the final mass and spin for GW170104 and GW150914, as well as the combined posterior. The difference in the estimates are divided by the mean of the two estimates to produce the fractional parameters that describe potential departures from the GR predictions: $\Delta a_f/\bar{a}_f$ for the spin and $\Delta M_f/\bar{M}_f$ for the mass [179]. These definitions are slightly different from the ones used in our earlier papers [7, 178], but serve the same qualitative role [179]. Each of the distributions is consistent with the GR value. The posterior for GW170104 is broader, consistent with this event being quieter, and having a lower total mass, which makes it harder to measure the post-inspiral parameters. The width of the 90% credible intervals for the combined posteriors of $\Delta M_f/\bar{M}_f$ are smaller than those computed from GW170104 (GW150914) by a factor of ~ 1.6 (1.3), and the intervals for $\Delta a_f/\bar{a}_f$ are improved by a factor of ~ 1.4 (1.2).

-
- [1] J. Aasi *et al.* (LIGO Scientific Collaboration), Classical Quantum Gravity **32**, 074001 (2015), arXiv:1411.4547 [gr-qc].
 - [2] B. P. Abbott *et al.* (LIGO Scientific Collaboration, Virgo Collaboration), Phys. Rev. Lett. **116**, 061102 (2016), arXiv:1602.03837 [gr-qc].
 - [3] B. Abbott *et al.* (LIGO Scientific Collaboration, Virgo Collaboration), Phys. Rev. Lett. **116**, 241103 (2016), arXiv:1606.04855 [gr-qc].
 - [4] B. P. Abbott *et al.* (LIGO Scientific Collaboration, Virgo Collaboration), Phys. Rev. D **93**, 122003 (2016), arXiv:1602.03839 [gr-qc].
 - [5] B. P. Abbott *et al.* (LIGO Scientific Collaboration, Virgo Collaboration), Phys. Rev. X **6**, 041015 (2016), arXiv:1606.04856 [gr-qc].
 - [6] B. P. Abbott *et al.* (LIGO Scientific Collaboration, Virgo Collaboration), Astrophys. J. Lett. **818**, L22 (2016), arXiv:1602.03846 [astro-ph.HE].
 - [7] B. P. Abbott *et al.* (LIGO Scientific Collaboration, Virgo Collaboration), Phys. Rev. Lett. **116**, 221101 (2016), arXiv:1602.03841 [gr-qc].
 - [8] B. P. Abbott *et al.* (LIGO Scientific Collaboration, Virgo Collaboration), Astrophys. J. Lett. **833**, L1 (2016), arXiv:1602.03842 [astro-ph.HE].
 - [9] S. Chatterji, L. Blackburn, G. Martin, and E. Katsavounidis, Classical Quantum Gravity **21**, S1809 (2004), arXiv:gr-qc/0412119 [gr-qc].
 - [10] B. P. Abbott *et al.* (Virgo, LIGO Scientific), Phys. Rev. Lett. **116**, 131103 (2016), arXiv:1602.03838 [gr-qc].
 - [11] See *Supplemental Material* at link.aps.org/supplemental/10.1103/PhysRevLett.118.221101 for technical details and additional results. This is included as an appendix of the arXiv version, and hence numbering differs from the journal version.
 - [12] S. Karki *et al.*, Rev. Sci. Instrum. **87**, 114503 (2016), arXiv:1608.05055 [astro-ph.IM].
 - [13] B. P. Abbott *et al.* (LIGO Scientific Collaboration), Phys. Rev. D **95**, 062003 (2017), arXiv:1602.03845 [gr-qc].
 - [14] B. P. Abbott *et al.* (LIGO Scientific Collaboration, Virgo Collaboration), Classical Quantum Gravity **33**, 134001 (2016), arXiv:1602.03844 [gr-qc].
 - [15] T. Dal Canton *et al.*, Phys. Rev. D **90**, 082004 (2014), arXiv:1405.6731 [gr-qc].
 - [16] S. A. Usman *et al.*, Classical Quantum Gravity **33**, 215004 (2016), arXiv:1508.02357 [gr-qc].
 - [17] A. H. Nitz, I. W. Harry, J. L. Willis, C. M. Biwer, D. A. Brown, L. P. Pekowsky, T. Dal Canton, A. R. Williamson, T. Dent, C. D. Capano, T. J. Massinger, A. K. Lenon, A. B. Nielsen, and M. Cabero, “PyCBC Software,” github.com/ligo-cbc/pycbc (2017).
 - [18] L. P. Singer and L. R. Price, Phys. Rev. D **93**, 024013 (2016), arXiv:1508.03634 [gr-qc].
 - [19] L. P. Singer *et al.*, Astrophys. J. Lett. **829**, L15 (2016), arXiv:1603.07333 [astro-ph.HE].
 - [20] LIGO Scientific Collaboration and Virgo Collaboration, Gamma-ray Coordinates Network/Transient Astronomy Network Circular **20364** (2017).

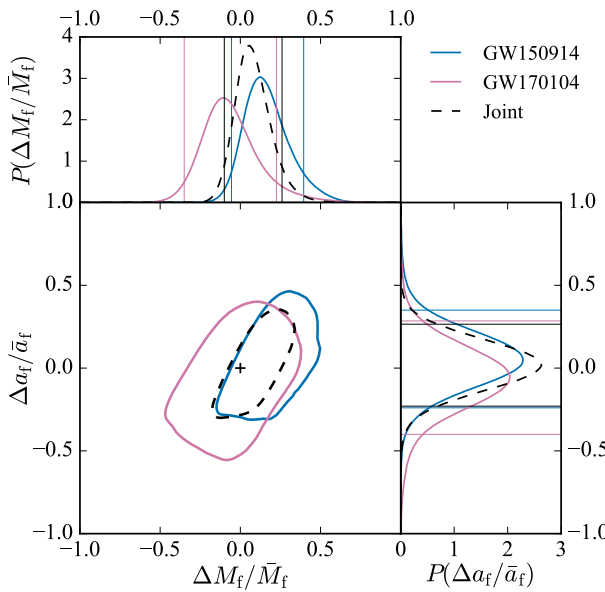


FIG. 15. Posterior probability distributions for the fractional differences in the remnant black hole mass $\Delta M_f/\bar{M}_f$ and spin $\Delta a_f/\bar{a}_f$ calculated using the low-frequency (inspiral) and high-frequency (merger–ringdown) parts of the waveform. The GR solution is at $(0, 0)$, shown in the two-dimensional plot as a black + marker. The contours show the 90% credible region, the lines in the one-dimensional histograms mark the 90% credible interval. We show the posteriors for GW170104 and GW150914, as well as the combined posterior using both.

- [21] The collection of Circulars exchanged with collaborating astronomers regarding this event is archived at gcn.gsfc.nasa.gov/other/G268556.gcn3.
- [22] C. Messick *et al.*, Phys. Rev. D **95**, 042001 (2017), arXiv:1604.04324 [astro-ph.IM].
- [23] C. Capano, I. Harry, S. Privitera, and A. Buonanno, Phys. Rev. D **93**, 124007 (2016), arXiv:1602.03509 [gr-qc].
- [24] D. A. Brown, I. Harry, A. Lundgren, and A. H. Nitz, Phys. Rev. D **86**, 084017 (2012), arXiv:1207.6406 [gr-qc].
- [25] I. W. Harry, B. Allen, and B. S. Sathyaprakash, Phys. Rev. D **80**, 104014 (2009), arXiv:0908.2090 [gr-qc].
- [26] P. Ajith, N. Fotopoulos, S. Privitera, A. Neunzert, N. Mazumder, and A. J. Weinstein, Phys. Rev. D **89**, 084041 (2014), arXiv:1210.6666 [gr-qc].
- [27] B. S. Sathyaprakash and S. V. Dhurandhar, Phys. Rev. D **44**, 3819 (1991).
- [28] B. J. Owen and B. S. Sathyaprakash, Phys. Rev. D **60**, 022002 (1999), arXiv:gr-qc/9808076 [gr-qc].
- [29] A. Bohé *et al.*, Phys. Rev. D **95**, 044028 (2017), arXiv:1611.03703 [gr-qc].
- [30] T. Dal Canton and I. Harry, (2017), arXiv:1705.01845 [gr-qc].
- [31] A. H. Nitz, T. Dent, T. Dal Canton, S. Fairhurst, and D. Brown, (2017), arXiv:1705.01513 [gr-qc].
- [32] B. P. Abbott *et al.* (LIGO Scientific Collaboration, Virgo Collaboration), Astrophys. J. Suppl. **227**, 14 (2016), arXiv:1606.03939 [astro-ph.HE].

- [33] W. M. Farr, J. R. Gair, I. Mandel, and C. Cutler, Phys. Rev. D **91**, 023005 (2015), arXiv:1302.5341 [astro-ph.IM].
- [34] B. P. Abbott *et al.* (LIGO Scientific Collaboration, Virgo Collaboration), Phys. Rev. D **93**, 122004 (2016), [Addendum: Phys. Rev.D **94**, 069903 (2016)], arXiv:1602.03843 [gr-qc].
- [35] S. Klimenko *et al.*, Phys. Rev. D **93**, 042004 (2016), arXiv:1511.05999 [gr-qc].
- [36] J. Veitch *et al.*, Phys. Rev. D **91**, 042003 (2015), arXiv:1409.7215 [gr-qc].
- [37] B. P. Abbott *et al.* (LIGO Scientific Collaboration, Virgo Collaboration), Phys. Rev. Lett. **116**, 241102 (2016), arXiv:1602.03840 [gr-qc].
- [38] M. Hannam, P. Schmidt, A. Bohé, L. Haegel, S. Husa, F. Ohme, G. Pratten, and M. Pürrer, Phys. Rev. Lett. **113**, 151101 (2014), arXiv:1308.3271 [gr-qc].
- [39] P. Schmidt, F. Ohme, and M. Hannam, Phys. Rev. D **91**, 024043 (2015), arXiv:1408.1810 [gr-qc].
- [40] S. Khan, S. Husa, M. Hannam, F. Ohme, M. Pürrer, X. Jiménez Forteza, and A. Bohé, Phys. Rev. D **93**, 044007 (2016), arXiv:1508.07253 [gr-qc].
- [41] Y. Pan, A. Buonanno, A. Taracchini, L. E. Kidder, A. H. Mroué, H. P. Pfeiffer, M. A. Scheel, and B. Szilágyi, Phys. Rev. D **89**, 084006 (2014), arXiv:1307.6232 [gr-qc].
- [42] A. Taracchini *et al.*, Phys. Rev. D **89**, 061502 (2014), arXiv:1311.2544 [gr-qc].
- [43] S. Babak, A. Taracchini, and A. Buonanno, Phys. Rev. D **95**, 024010 (2017), arXiv:1607.05661 [gr-qc].
- [44] B. Abbott *et al.* (LIGO Scientific Collaboration, Virgo Collaboration), Phys. Rev. X **6**, 041014 (2016), arXiv:1606.01210 [gr-qc].
- [45] F. Hofmann, E. Barausse, and L. Rezzolla, Astrophys. J. Lett. **825**, L19 (2016), arXiv:1605.01938 [gr-qc].
- [46] X. Jiménez-Forteza, D. Keitel, S. Husa, M. Hannam, S. Khan, and M. Pürrer, Phys. Rev. D **95**, 064024 (2017), arXiv:1611.00332 [gr-qc].
- [47] J. Healy and C. O. Lousto, Phys. Rev. D **95**, 024037 (2017), arXiv:1610.09713 [gr-qc].
- [48] N. K. Johnson-McDaniel *et al.*, *Determining the final spin of a binary black hole system including in-plane spins: Method and checks of accuracy*, Tech. Rep. LIGO-T1600168 (LIGO Scientific Collaboration and Virgo Collaboration, 2016).
- [49] D. Keitel *et al.*, (2016), arXiv:1612.09566 [gr-qc].
- [50] A. Krolak and B. F. Schutz, Gen. Relativ. Gravit. **19**, 1163 (1987).
- [51] D. E. Holz and S. A. Hughes, Astrophys. J. **629**, 15 (2005), arXiv:astro-ph/0504616 [astro-ph].
- [52] P. A. R. Ade *et al.* (Planck Collaboration), Astron. Astrophys. **594**, A13 (2016), arXiv:1502.01589 [astro-ph.CO].
- [53] P. Ajith and S. Bose, Phys. Rev. D **79**, 084032 (2009), arXiv:0901.4936 [gr-qc].
- [54] J. Veitch, M. Pürrer, and I. Mandel, Phys. Rev. Lett. **115**, 141101 (2015), arXiv:1503.05953 [astro-ph.HE].
- [55] P. B. Graff, A. Buonanno, and B. S. Sathyaprakash, Phys. Rev. D **92**, 022002 (2015), arXiv:1504.04766 [gr-qc].
- [56] C.-J. Haster, Z. Wang, C. P. L. Berry, S. Stevenson, J. Veitch, and I. Mandel, Mon. Not. R. Astron. Soc. **457**, 4499 (2016), arXiv:1511.01431 [astro-ph.HE].

- [57] A. Ghosh, W. Del Pozzo, and P. Ajith, Phys. Rev. D **94**, 104070 (2016), arXiv:1505.05607 [gr-qc].
- [58] L. S. Finn and D. F. Chernoff, Phys. Rev. D **47**, 2198 (1993), arXiv:gr-qc/9301003 [gr-qc].
- [59] C. Cutler and É. E. Flanagan, Phys. Rev. D **49**, 2658 (1994), arXiv:gr-qc/9402014 [gr-qc].
- [60] L. Blanchet, T. Damour, B. R. Iyer, C. M. Will, and A. G. Wiseman, Phys. Rev. Lett. **74**, 3515 (1995), arXiv:gr-qc/9501027 [gr-qc].
- [61] S. Vitale, R. Lynch, J. Veitch, V. Raymond, and R. Sturani, Phys. Rev. Lett. **112**, 251101 (2014), arXiv:1403.0129 [gr-qc].
- [62] T. A. Apostolatos, C. Cutler, G. J. Sussman, and K. S. Thorne, Phys. Rev. D **49**, 6274 (1994).
- [63] L. Blanchet, Living Rev. Relativity **17**, 2 (2014), arXiv:1310.1528 [gr-qc].
- [64] T. Damour, Phys. Rev. D **64**, 124013 (2001), arXiv:gr-qc/0103018 [gr-qc].
- [65] P. Ajith *et al.*, Phys. Rev. Lett. **106**, 241101 (2011), arXiv:0909.2867 [gr-qc].
- [66] L. Santamaría *et al.*, Phys. Rev. D **82**, 064016 (2010), arXiv:1005.3306 [gr-qc].
- [67] M. Campanelli, C. O. Lousto, and Y. Zlochower, Phys. Rev. D **74**, 041501 (2006), arXiv:gr-qc/0604012 [gr-qc].
- [68] C. Reisswig, S. Husa, L. Rezzolla, E. N. Dorband, D. Pollney, and J. Seiler, Phys. Rev. D **80**, 124026 (2009), arXiv:0907.0462 [gr-qc].
- [69] M. Pürrer, M. Hannam, P. Ajith, and S. Husa, Phys. Rev. D **88**, 064007 (2013), arXiv:1306.2320 [gr-qc].
- [70] M. Pürrer, M. Hannam, and F. Ohme, Phys. Rev. D **93**, 084042 (2016), arXiv:1512.04955 [gr-qc].
- [71] S. Vitale, R. Lynch, V. Raymond, R. Sturani, J. Veitch, and P. Graff, Phys. Rev. D **95**, 064053 (2017), arXiv:1611.01122 [gr-qc].
- [72] É. Racine, Phys. Rev. D **78**, 044021 (2008), arXiv:0803.1820 [gr-qc].
- [73] D. Gerosa, M. Kesden, U. Sperhake, E. Berti, and R. O’Shaughnessy, Phys. Rev. D **92**, 064016 (2015), arXiv:1506.03492 [gr-qc].
- [74] B. F. Schutz, Nature **323**, 310 (1986).
- [75] S. Nissanke, D. E. Holz, S. A. Hughes, N. Dalal, and J. L. Sievers, Astrophys. J. **725**, 496 (2010), arXiv:0904.1017 [astro-ph.CO].
- [76] C. L. Rodriguez, B. Farr, V. Raymond, W. M. Farr, T. B. Littenberg, D. Fazi, and V. Kalogera, Astrophys. J. **784**, 119 (2014), arXiv:1309.3273 [astro-ph.HE].
- [77] B. Farr *et al.*, Astrophys. J. **825**, 116 (2016), arXiv:1508.05336 [astro-ph.HE].
- [78] B. P. Abbott *et al.* (LIGO Scientific Collaboration, Virgo Collaboration), Classical Quantum Gravity **34**, 104002 (2017), arXiv:1611.07531 [gr-qc].
- [79] B. P. Abbott *et al.* (LIGO Scientific Collaboration, Virgo Collaboration), Phys. Rev. D **94**, 064035 (2016), arXiv:1606.01262 [gr-qc].
- [80] V. Varma, P. Ajith, S. Husa, J. C. Bustillo, M. Hannam, and M. Pürrer, Phys. Rev. D **90**, 124004 (2014), arXiv:1409.2349 [gr-qc].
- [81] J. Calderón Bustillo, S. Husa, A. M. Sintes, and M. Pürrer, Phys. Rev. D **93**, 084019 (2016), arXiv:1511.02060 [gr-qc].
- [82] N. J. Cornish and T. B. Littenberg, Classical Quantum Gravity **32**, 135012 (2015), arXiv:1410.3835 [gr-qc].
- [83] E. E. Salpeter, Astrophys. J. **121**, 161 (1955).
- [84] S. F. Portegies Zwart and S. McMillan, Astrophys. J. Lett. **528**, L17 (2000), arXiv:astro-ph/9910061 [astro-ph].
- [85] C. L. Rodriguez, C.-J. Haster, S. Chatterjee, V. Kalogera, and F. A. Rasio, Astrophys. J. Lett. **824**, L8 (2016), arXiv:1604.04254 [astro-ph.HE].
- [86] R. M. O’Leary, Y. Meiron, and B. Kocsis, Astrophys. J. Lett. **824**, L12 (2016), arXiv:1602.02809 [astro-ph.HE].
- [87] M. Mapelli, Mon. Not. R. Astron. Soc. **459**, 3432 (2016), arXiv:1604.03559 [astro-ph.GA].
- [88] S. Banerjee, Mon. Not. R. Astron. Soc. **467**, 524 (2017), arXiv:1611.09357 [astro-ph.HE].
- [89] J. R. Hurley, A. C. Sippel, C. A. Tout, and S. J. Aarseth, Publ. Astron. Soc. Aust. **33**, e036 (2016), arXiv:1607.00641 [astro-ph.GA].
- [90] A. Askar, M. Szkludlarek, D. Gondek-Rosińska, M. Giersz, and T. Bulik, Mon. Not. R. Astron. Soc. Lett. **464**, L36 (2017), arXiv:1608.02520 [astro-ph.HE].
- [91] D. Park, C. Kim, H. M. Lee, Y.-B. Bae, and C. Belczynski, Mon. Not. R. Astron. Soc. (2017), 10.1093/mnras/stx1015, arXiv:1703.01568 [astro-ph.HE].
- [92] N. C. Stone, B. D. Metzger, and Z. Haiman, Mon. Not. R. Astron. Soc. **464**, 946 (2017), arXiv:1602.04226 [astro-ph.GA].
- [93] I. Bartos, B. Kocsis, Z. Haiman, and S. Márka, Astrophys. J. **835**, 165 (2017), arXiv:1602.03831 [astro-ph.HE].
- [94] F. Antonini and F. A. Rasio, Astrophys. J. **831**, 187 (2016), arXiv:1606.04889 [astro-ph.HE].
- [95] K. Silsbee and S. Tremaine, Astrophys. J. **836**, 39 (2017), arXiv:1608.07642 [astro-ph.HE].
- [96] F. Antonini, S. Toonen, and A. S. Hamers, (2017), arXiv:1703.06614 [astro-ph.GA].
- [97] A. Tutukov and L. Yungelson, Nauchnye Informatsii **27**, 70 (1973).
- [98] R. Voss and T. M. Tauris, Mon. Not. R. Astron. Soc. **342**, 1169 (2003), arXiv:astro-ph/0303227 [astro-ph].
- [99] N. Mennekens and D. Vanbeveren, Astron. Astrophys. **564**, A134 (2014), arXiv:1307.0959 [astro-ph.SR].
- [100] K. Belczynski, D. E. Holz, T. Bulik, and R. O’Shaughnessy, Nature **534**, 512 (2016), arXiv:1602.04531 [astro-ph.HE].
- [101] J. J. Eldridge and E. R. Stanway, Mon. Not. R. Astron. Soc. **462**, 3302 (2016), arXiv:1602.03790 [astro-ph.HE].
- [102] V. M. Lipunov, V. Kornilov, E. Gorbovskoy, N. Tiurina, P. Balanutsa, and A. Kuznetsov, New Astron. **51**, 122 (2017), arXiv:1605.01604 [astro-ph.HE].
- [103] S. E. Woosley, Astrophys. J. Lett. **824**, L10 (2016), arXiv:1603.00511 [astro-ph.HE].
- [104] M. U. Kruckow, T. M. Tauris, N. Langer, D. Szécsi, P. Marchant, and P. Podsiadlowski, Astron. Astrophys. **596**, A58 (2016), arXiv:1610.04417 [astro-ph.SR].
- [105] S. Stevenson, A. Vigna-Gómez, I. Mandel, J. W. Barrett, C. J. Neijssel, D. Perkins, and S. E. de Mink, Nature Commun. **8**, 14906 (2017), arXiv:1704.01352 [astro-ph.HE].
- [106] P. Marchant, N. Langer, P. Podsiadlowski, T. M. Tauris, and T. J. Moriya, Astron. Astrophys. **588**, A50 (2016), arXiv:1601.03718 [astro-ph.SR].
- [107] I. Mandel and S. E. de Mink, Mon. Not. R. Astron. Soc. **458**, 2634 (2016), arXiv:1601.00007 [astro-ph.HE].
- [108] K. Pavlovskii, N. Ivanova, K. Belczynski, and K. X. Van, Mon. Not. R. Astron. Soc. **465**, 2092 (2017), arXiv:1606.04921 [astro-ph.HE].

- [109] E. P. J. van den Heuvel, S. F. Portegies Zwart, and S. E. de Mink, (2017), arXiv:1701.02355 [astro-ph.SR].
- [110] T. Hartwig, M. Volonteri, V. Bromm, R. S. Klessen, E. Barausse, M. Magg, and A. Stacy, Mon. Not. R. Astron. Soc. Lett. **460**, L74 (2016), arXiv:1603.05655 [astro-ph.GA].
- [111] K. Inayoshi, R. Hirai, T. Kinugawa, and K. Hotokezaka, (2017), arXiv:1701.04823 [astro-ph.HE].
- [112] J. S. Vink, New Astron. Rev. **52**, 419 (2008).
- [113] K. Belczynski, T. Bulik, C. L. Fryer, A. Ruiter, J. S. Vink, and J. R. Hurley, Astrophys. J. **714**, 1217 (2010), arXiv:0904.2784 [astro-ph.SR].
- [114] M. Spera, M. Mapelli, and A. Bressan, Mon. Not. R. Astron. Soc. **451**, 4086 (2015), arXiv:1505.05201 [astro-ph.SR].
- [115] C. L. Rodriguez, S. Chatterjee, and F. A. Rasio, Phys. Rev. D **93**, 084029 (2016), arXiv:1602.02444 [astro-ph.HE].
- [116] V. Petit, Z. Keszthelyi, R. MacInnis, D. H. Cohen, R. H. D. Townsend, G. A. Wade, S. L. Thomas, S. P. Owocki, J. Puls, and J. A. ud-Doula, Mon. Not. R. Astron. Soc. **466**, 1052 (2017), arXiv:1611.08964 [astro-ph.SR].
- [117] B. J. Carr and S. W. Hawking, Mon. Not. R. Astron. Soc. **168**, 399 (1974).
- [118] S. Bird, I. Cholis, J. B. Muñoz, Y. Ali-Haïmoud, M. Kamionkowski, E. D. Kovetz, A. Raccaelli, and A. G. Riess, Phys. Rev. Lett. **116**, 201301 (2016), arXiv:1603.00464 [astro-ph.CO].
- [119] S. Clesse and J. García-Bellido, Phys. Dark Univ. **15**, 142 (2017), arXiv:1603.05234 [astro-ph.CO].
- [120] B. Carr, F. Künnel, and M. Sandstad, Phys. Rev. D **94**, 083504 (2016), arXiv:1607.06077 [astro-ph.CO].
- [121] M. Sasaki, T. Suyama, T. Tanaka, and S. Yokoyama, Phys. Rev. Lett. **117**, 061101 (2016), arXiv:1603.08338 [astro-ph.CO].
- [122] M. Ricotti, J. P. Ostriker, and K. J. Mack, Astrophys. J. **680**, 829 (2008), arXiv:0709.0524 [astro-ph].
- [123] S. Clesse and J. García-Bellido, Phys. Rev. D **92**, 023524 (2015), arXiv:1501.07565 [astro-ph.CO].
- [124] A. Kashlinsky, Astrophys. J. Lett. **823**, L25 (2016), arXiv:1605.04023 [astro-ph.CO].
- [125] A. M. Green, Phys. Rev. D **94**, 063530 (2016), arXiv:1609.01143 [astro-ph.CO].
- [126] Y. Ali-Haïmoud and M. Kamionkowski, Phys. Rev. D **95**, 043534 (2017), arXiv:1612.05644 [astro-ph.CO].
- [127] E. Mediavilla, J. Jiménez-Vicente, J. A. Muñoz, H. Vives-Arias, and J. Calderón-Infante, Astrophys. J. Lett. **836**, L18 (2017), arXiv:1702.00947 [astro-ph.GA].
- [128] B. Carr, M. Raidal, T. Tenkanen, V. Vaskonen, and H. Veermäe, (2017), arXiv:1705.05567 [astro-ph.CO].
- [129] C. L. Rodriguez, M. Zevin, C. Pankow, V. Kalogera, and F. A. Rasio, Astrophys. J. Lett. **832**, L2 (2016), arXiv:1609.05916 [astro-ph.HE].
- [130] V. Kalogera, Astrophys. J. **541**, 319 (2000), arXiv:astro-ph/9911417 [astro-ph].
- [131] J. M. Bardeen and J. A. Petterson, Astrophys. J. Lett. **195**, L65 (1975).
- [132] A. R. King, S. H. Lubow, G. I. Ogilvie, and J. E. Pringle, Mon. Not. R. Astron. Soc. **363**, 49 (2005), arXiv:astro-ph/0507098 [astro-ph].
- [133] J. P. Zahn, Astron. Astrophys. **57**, 383 (1977).
- [134] P. Hut, Astron. Astrophys. **99**, 126 (1981).
- [135] R. O’Shaughnessy, D. Gerosa, and D. Wysocki, (2017), arXiv:1704.03879 [astro-ph.HE].
- [136] R. G. Martin, C. A. Tout, and J. E. Pringle, Mon. Not. R. Astron. Soc. **401**, 1514 (2010), arXiv:0910.0018 [astro-ph.HE].
- [137] T.-W. Wong, F. Valsecchi, A. Ansari, T. Fragos, E. Glebbeek, V. Kalogera, and J. McClintonck, Astrophys. J. **790**, 119 (2014), arXiv:1304.3756 [astro-ph.HE].
- [138] H.-T. Janka, Mon. Not. R. Astron. Soc. **434**, 1355 (2013), arXiv:1306.0007 [astro-ph.SR].
- [139] S. Repetto and G. Nelemans, Mon. Not. R. Astron. Soc. **453**, 3341 (2015), arXiv:1507.08105 [astro-ph.HE].
- [140] I. Mandel, Mon. Not. R. Astron. Soc. **456**, 578 (2016), arXiv:1510.03871 [astro-ph.HE].
- [141] S. Repetto, A. P. Igoshhev, and G. Nelemans, Mon. Not. R. Astron. Soc. **467**, 298 (2017), arXiv:1701.01347 [astro-ph.HE].
- [142] M. Dominik, K. Belczynski, C. Fryer, D. E. Holz, E. Berti, T. Bulik, I. Mandel, and R. O’Shaughnessy, Astrophys. J. **779**, 72 (2013), arXiv:1308.1546 [astro-ph.HE].
- [143] H. Spruit and E. S. Phinney, Nature **393**, 139 (1998), arXiv:astro-ph/9803201 [astro-ph].
- [144] W. M. Farr, K. Kremer, M. Lyutikov, and V. Kalogera, Astrophys. J. **742**, 81 (2011), arXiv:1104.5001 [astro-ph.HE].
- [145] R. D. Ferdman *et al.*, Astrophys. J. **767**, 85 (2013), arXiv:1302.2914 [astro-ph.SR].
- [146] R. Kazeroni, J. Guilet, and T. Foglizzo, (2017), arXiv:1701.07029 [astro-ph.HE].
- [147] M. C. Miller and J. M. Miller, Phys. Rept. **548**, 1 (2015), arXiv:1408.4145 [astro-ph.HE].
- [148] T. Fragos and J. E. McClintonck, Astrophys. J. **800**, 17 (2015), arXiv:1408.2661 [astro-ph.HE].
- [149] J. Fuller, M. Cantiello, D. Lecoanet, and E. Quataert, Astrophys. J. **810**, 101 (2015), [Erratum: Astrophys. J. **815**, 137 (2015)], arXiv:1502.07779 [astro-ph.SR].
- [150] M. Zaldarriaga, D. Kushnir, and J. A. Kollmeier, (2017), arXiv:1702.00885 [astro-ph.HE].
- [151] K. Hotokezaka and T. Piran, (2017), arXiv:1702.03952 [astro-ph.HE].
- [152] D. Gerosa, M. Kesden, E. Berti, R. O’Shaughnessy, and U. Sperhake, Phys. Rev. D **87**, 104028 (2013), arXiv:1302.4442 [gr-qc].
- [153] W. M. Farr, S. Stevenson, M. C. Miller, A. Vecchio, and I. Mandel, *Distinguishing Spin-Aligned and Isotropic Black Hole Populations With Gravitational Waves*, Tech. Rep. LIGO-P1700067 (2017).
- [154] D. Gerosa, R. O’Shaughnessy, M. Kesden, E. Berti, and U. Sperhake, Phys. Rev. D **89**, 124025 (2014), arXiv:1403.7147 [gr-qc].
- [155] S. Vitale, R. Lynch, R. Sturani, and P. Graff, Classical Quantum Gravity **34**, 03LT01 (2017), arXiv:1503.04307 [gr-qc].
- [156] D. Gerosa and E. Berti, (2017), arXiv:1703.06223 [gr-qc].
- [157] M. Fishbach, D. E. Holz, and B. Farr, Astrophys. J. Lett. **840**, L24 (2017), arXiv:1703.06869 [astro-ph.HE].
- [158] S. Stevenson, C. P. L. Berry, and I. Mandel, (2017), arXiv:1703.06873 [astro-ph.HE].
- [159] C. Talbot and E. Thrane, (2017), arXiv:1704.08370 [astro-ph.HE].

- [160] S. Mirshekari, N. Yunes, and C. M. Will, Phys. Rev. D **85**, 024041 (2012), arXiv:1110.2720 [gr-qc].
- [161] N. Yunes, K. Yagi, and F. Pretorius, Phys. Rev. D **94**, 084002 (2016), arXiv:1603.08955 [gr-qc].
- [162] D. Mattingly, Living Rev. Relativity **8**, 5 (2005), arXiv:gr-qc/0502097 [gr-qc].
- [163] C. M. Will, Living Rev. Relativity **17**, 4 (2014), arXiv:1403.7377 [gr-qc].
- [164] G. Calcagni, Phys. Rev. Lett. **104**, 251301 (2010), arXiv:0912.3142 [hep-th].
- [165] G. Amelino-Camelia, Nature **418**, 34 (2002), arXiv:gr-qc/0207049 [gr-qc].
- [166] P. Hořava, Phys. Rev. D **79**, 084008 (2009), arXiv:0901.3775 [hep-th].
- [167] A. S. Sefiedgar, K. Nozari, and H. R. Sepangi, Phys. Lett. B **696**, 119 (2011), arXiv:1012.1406 [gr-qc].
- [168] M. D. Seifert, Phys. Rev. D **81**, 065010 (2010), arXiv:0909.3118 [hep-ph].
- [169] B. Altschul, Q. G. Bailey, and V. A. Kostelecky, Phys. Rev. D **81**, 065028 (2010), arXiv:0912.4852 [gr-qc].
- [170] C. M. Will, Phys. Rev. D **57**, 2061 (1998), arXiv:gr-qc/9709011 [gr-qc].
- [171] L. Blanchet, T. Damour, G. Esposito-Farèse, and B. R. Iyer, Phys. Rev. Lett. **93**, 091101 (2004), arXiv:gr-qc/0406012 [gr-qc].
- [172] L. Blanchet and B. S. Sathyaprakash, Classical Quantum Gravity **11**, 2807 (1994).
- [173] L. Blanchet, T. Damour, and B. R. Iyer, Phys. Rev. D **51**, 5360 (1995), [Erratum: Phys. Rev. D **54**, 1860 (1996)], arXiv:gr-qc/9501029 [gr-qc].
- [174] K. G. Arun, B. R. Iyer, M. S. S. Qusailah, and B. S. Sathyaprakash, Phys. Rev. D **74**, 024006 (2006), arXiv:gr-qc/0604067 [gr-qc].
- [175] C. K. Mishra, K. G. Arun, B. R. Iyer, and B. S. Sathyaprakash, Phys. Rev. D **82**, 064010 (2010), arXiv:1005.0304 [gr-qc].
- [176] N. Yunes and F. Pretorius, Phys. Rev. D **80**, 122003 (2009), arXiv:0909.3328 [gr-qc].
- [177] T. G. F. Li, W. Del Pozzo, S. Vitale, C. Van Den Broeck, M. Agathos, J. Veitch, K. Grover, T. Sidery, R. Sturani, and A. Vecchio, Phys. Rev. D **85**, 082003 (2012), arXiv:1110.0530 [gr-qc].
- [178] A. Ghosh *et al.*, Phys. Rev. D **94**, 021101 (2016), arXiv:1602.02453 [gr-qc].
- [179] A. Ghosh, N. K. Johnson-McDaniel, A. Ghosh, C. K. Mishra, P. Ajith, W. Del Pozzo, C. P. L. Berry, A. B. Nielsen, and L. London, (2017), arXiv:1704.06784 [gr-qc].
- [180] LIGO Scientific Collaboration, “LIGO Open Science Center release of GW170104,” doi.org/10.7935/K53X84K2 (2017).
- [181] J. Kissel, J. Betzwieser, X. Siemens, R. Savage, K. Kawabe, M. Wade, B. O’Reilly, K. Izumi, S. Karki, D. Tuyenbayev, D. Martynov, S. Kandhasamy, M. Fays, and C. Cahillane, *Advanced LIGO Sensitivity Plots*, Tech. Rep. LIGO-G1500623 (LIGO Scientific Collaboration, 2016).
- [182] K. Cannon, C. Hanna, and J. Peoples, (2015), arXiv:1504.04632 [astro-ph.IM].
- [183] W. M. Farr, B. Farr, and T. Littenberg, *Modelling Calibration Errors In CBC Waveforms*, Tech. Rep. LIGO-T1400682 (LIGO Scientific Collaboration and Virgo Collaboration, 2015).
- [184] LIGO Scientific Collaboration and Virgo Collaboration, Gamma-ray Coordinates Network/Transient Astronomy Network Circular **20385** (2017).
- [185] R. Smith, S. E. Field, K. Blackburn, C.-J. Haster, M. Pürrer, V. Raymond, and P. Schmidt, Phys. Rev. D **94**, 044031 (2016), arXiv:1604.08253 [gr-qc].
- [186] S. Husa, S. Khan, M. Hannam, M. Pürrer, F. Ohme, X. J. Forteza, and A. Bohé, Phys. Rev. D **93**, 044006 (2016), arXiv:1508.07250 [gr-qc].
- [187] T. B. Littenberg and N. J. Cornish, Phys. Rev. D **91**, 084034 (2015), arXiv:1410.3852 [gr-qc].
- [188] B. Farr, E. Ochsner, W. M. Farr, and R. O’Shaughnessy, Phys. Rev. D **90**, 024018 (2014), arXiv:1404.7070 [gr-qc].
- [189] B. F. Schutz, Classical Quantum Gravity **28**, 125023 (2011), arXiv:1102.5421 [astro-ph.IM].
- [190] S. Nissanke, M. Kasliwal, and A. Georgieva, Astrophys. J. **767**, 124 (2013), arXiv:1210.6362 [astro-ph.HE].
- [191] S. Kullback and R. A. Leibler, Ann. Math. Statist. **22**, 79 (1951).
- [192] D. J. C. MacKay, *Information Theory, Inference and Learning Algorithms* (Cambridge University Press, Cambridge, 2003).
- [193] I. Mandel and R. O’Shaughnessy, Classical Quantum Gravity **27**, 114007 (2010), arXiv:0912.1074 [astro-ph.HE].
- [194] J. A. Gonzalez, U. Sperhake, B. Bruegmann, M. Hannam, and S. Husa, Phys. Rev. Lett. **98**, 091101 (2007), arXiv:gr-qc/0610154 [gr-qc].
- [195] E. Berti, V. Cardoso, J. A. Gonzalez, U. Sperhake, M. Hannam, S. Husa, and B. Bruegmann, Phys. Rev. D **76**, 064034 (2007), arXiv:gr-qc/0703053 [GR-QC].
- [196] F. Özel, D. Psaltis, R. Narayan, and J. E. McClintock, Astrophys. J. **725**, 1918 (2010), arXiv:1006.2834 [astro-ph.GA].
- [197] W. M. Farr, N. Sravan, A. Cantrell, L. Kreidberg, C. D. Bailyn, I. Mandel, and V. Kalogera, Astrophys. J. **741**, 103 (2011), arXiv:1011.1459 [astro-ph.GA].
- [198] L. Kreidberg, C. D. Bailyn, W. M. Farr, and V. Kalogera, Astrophys. J. **757**, 36 (2012), arXiv:1205.1805 [astro-ph.HE].
- [199] P. Kroupa, Mon. Not. R. Astron. Soc. **322**, 231 (2001), arXiv:astro-ph/0009005 [astro-ph].
- [200] H. A. Kobulnicky and C. L. Fryer, Astrophys. J. **670**, 747 (2007).
- [201] H. Sana, S. E. de Mink, A. de Koter, N. Langer, C. J. Evans, M. Gieles, E. Gosset, R. G. Izzard, J. B. L. Bouquin, and F. R. N. Schneider, Science **337**, 444 (2012), arXiv:1207.6397 [astro-ph.SR].
- [202] H. A. Kobulnicky *et al.*, Astrophys. J. Suppl. **213**, 34 (2014), arXiv:1406.6655 [astro-ph.SR].
- [203] C. L. Fryer and V. Kalogera, Astrophys. J. **554**, 548 (2001), arXiv:astro-ph/9911312 [astro-ph].
- [204] C. L. Fryer, K. Belczynski, G. Wiktorowicz, M. Dominik, V. Kalogera, and D. E. Holz, Astrophys. J. **749**, 91 (2012), arXiv:1110.1726 [astro-ph.SR].
- [205] M. Dominik, K. Belczynski, C. Fryer, D. Holz, E. Berti, T. Bulik, I. Mandel, and R. O’Shaughnessy, Astrophys. J. **759**, 52 (2012), arXiv:1202.4901 [astro-ph.HE].
- [206] I. Mandel, Phys. Rev. D **81**, 084029 (2010), arXiv:0912.5531 [astro-ph.HE].
- [207] G. D. Moore and A. E. Nelson, J. High Energy Phys. **09**, 023 (2001), arXiv:hep-ph/0106220 [hep-ph].

- [208] E. Borriello, S. Chakraborty, A. Mirizzi, and P. D. Serpico, Phys. Rev. D **87**, 116009 (2013), arXiv:1303.5843 [astro-ph.HE].
- [209] S. Kiyota and K. Yamamoto, Phys. Rev. D **92**, 104036 (2015), arXiv:1509.00610 [gr-qc].
- [210] J.-J. Wei, B.-B. Zhang, L. Shao, X.-F. Wu, and P. Mészáros, Astrophys. J. Lett. **834**, L13 (2017), arXiv:1612.09425 [astro-ph.HE].
- [211] Z.-Y. Wang, R.-Y. Liu, and X.-Y. Wang, Phys. Rev. Lett. **116**, 151101 (2016), arXiv:1602.06805 [astro-ph.HE].
- [212] D. B. Rubin, Ann. Statist. **9**, 130 (1981).
- [213] M. Pürrer, Classical Quantum Gravity **31**, 195010 (2014), arXiv:1402.4146 [gr-qc].
- [214] F. Pretorius, Phys. Rev. Lett. **95**, 121101 (2005), arXiv:gr-qc/0507014 [gr-qc].
- [215] M. Campanelli, C. O. Lousto, P. Marronetti, and Y. Zlochower, Phys. Rev. Lett. **96**, 111101 (2006), arXiv:gr-qc/0511048 [gr-qc].
- [216] J. G. Baker, J. R. van Meter, S. T. McWilliams, J. Centrella, and B. J. Kelly, Phys. Rev. Lett. **99**, 181101 (2007), arXiv:gr-qc/0612024 [gr-qc].
- [217] C. V. Vishveshwara, Nature **227**, 936 (1970).
- [218] S. Chandrasekhar and S. L. Detweiler, Proc. Roy. Soc. Lond. A **344**, 441 (1975).
- [219] S. A. Teukolsky, Astrophys. J. **185**, 635 (1973).
- [220] K. D. Kokkotas and B. G. Schmidt, Living Rev. Relativity **2**, 2 (1999), arXiv:gr-qc/9909058 [gr-qc].
- [221] A. Buonanno and T. Damour, Phys. Rev. D **59**, 084006 (1999), arXiv:gr-qc/9811091 [gr-qc].
- [222] A. Buonanno and T. Damour, Phys. Rev. D **62**, 064015 (2000), arXiv:gr-qc/0001013 [gr-qc].
- [223] P. Ajith *et al.*, Classical Quantum Gravity **24**, S689 (2007), arXiv:0704.3764 [gr-qc].
- [224] A. H. Mroue *et al.*, Phys. Rev. Lett. **111**, 241104 (2013), arXiv:1304.6077 [gr-qc].
- [225] T. Chu, H. Fong, P. Kumar, H. P. Pfeiffer, M. Boyle, D. A. Hemberger, L. E. Kidder, M. A. Scheel, and B. Szilagyi, Classical Quantum Gravity **33**, 165001 (2016), arXiv:1512.06800 [gr-qc].
- [226] D. Psaltis, Living Rev. Relativity **11**, 9 (2008), arXiv:0806.1531 [astro-ph].
- [227] E. Berti *et al.*, Classical Quantum Gravity **32**, 243001 (2015), arXiv:1501.07274 [gr-qc].
- [228] B. Abbott *et al.* (LIGO Scientific Collaboration, Virgo Collaboration), Phys. Rev. Lett. **121**, 129901(E) (2018).

Authors

- B. P. Abbott,¹ R. Abbott,¹ T. D. Abbott,² F. Acernese,^{3,4} K. Ackley,⁵ C. Adams,⁶ T. Adams,⁷ P. Addesso,⁸ R. X. Adhikari,¹ V. B. Adya,⁹ C. Affeldt,⁹ M. Afrough,¹⁰ B. Agarwal,¹¹ M. Agathos,¹² K. Agatsuma,¹³ N. Aggarwal,¹⁴ O. D. Aguiar,¹⁵ L. Aiello,^{16,17} A. Ain,¹⁸ P. Ajith,¹⁹ B. Allen,^{9,20,21} G. Allen,¹¹ A. Allocca,^{22,23} P. A. Altin,²⁴ A. Amato,²⁵ A. Ananyeva,¹ S. B. Anderson,¹ W. G. Anderson,²⁰ S. Antier,²⁶ S. Appert,¹ K. Arai,¹ M. C. Araya,¹ J. S. Areeda,²⁷ N. Arnaud,^{26,28} K. G. Arun,²⁹ S. Ascenzi,^{30,17} G. Ashton,⁹ M. Ast,³¹ S. M. Aston,⁶ P. Astone,³² P. Aufmuth,²¹ C. Aulbert,⁹ K. AultONeal,³³ A. Avila-Alvarez,²⁷ S. Babak,³⁴ P. Bacon,³⁵ M. K. M. Bader,¹³ S. Bae,³⁶ P. T. Baker,^{37,38} F. Baldaccini,^{39,40} G. Ballardin,²⁸ S. W. Ballmer,⁴¹ S. Banagiri,⁴² J. C. Barayoga,¹ S. E. Barclay,⁴³ B. C. Barish,¹ D. Barker,⁴⁴ F. Barone,^{3,4} B. Barr,⁴³ L. Barsotti,¹⁴ M. Barsuglia,³⁵ D. Barta,⁴⁵ J. Bartlett,⁴⁴ I. Bartos,⁴⁶ R. Bassiri,⁴⁷ A. Basti,^{22,23} J. C. Batch,⁴⁴ C. Baune,⁹ M. Bawaj,^{48,40} M. Bazzan,^{49,50} B. Bécsy,⁵¹ C. Beer,⁹ M. Bejger,⁵² I. Belahcene,²⁶ A. S. Bell,⁴³ B. K. Berger,¹ G. Bergmann,⁹ C. P. L. Berry,⁵³ D. Bersanetti,^{54,55} A. Bertolini,¹³ J. Betzwieser,⁶ S. Bhagwat,⁴¹ R. Bhandare,⁵⁶ I. A. Bilenko,⁵⁷ G. Billingsley,¹ C. R. Billman,⁵ J. Birch,⁶ R. Birney,⁵⁸ O. Birnholtz,⁹ S. Biscans,¹⁴ A. Bisht,²¹ M. Bitossi,^{28,23} C. Biwer,⁴¹ M. A. Bizouard,²⁶ J. K. Blackburn,¹ J. Blackman,⁵⁹ C. D. Blair,⁶⁰ D. G. Blair,⁶⁰ R. M. Blair,⁴⁴ S. Bloemen,⁶¹ O. Bock,⁹ N. Bode,⁹ M. Boer,⁶² G. Bogaert,⁶² A. Bohe,³⁴ F. Bondu,⁶³ R. Bonnand,⁷ B. A. Boom,¹³ R. Bork,¹ V. Boschi,^{22,23} S. Bose,^{64,18} Y. Bouffanais,³⁵ A. Bozzi,²⁸ C. Bradaschia,²³ P. R. Brady,²⁰ V. B. Braginsky*,⁵⁷ M. Branchesi,^{65,66} J. E. Brau,⁶⁷ T. Briant,⁶⁸ A. Brillet,⁶² M. Brinkmann,⁹ V. Brisson,²⁶ P. Brockill,²⁰ J. E. Broida,⁶⁹ A. F. Brooks,¹ D. A. Brown,⁴¹ D. D. Brown,⁵³ N. M. Brown,¹⁴ S. Brunett,¹ C. C. Buchanan,² A. Buikema,¹⁴ T. Bulik,⁷⁰ H. J. Bulten,^{71,13} A. Buonanno,^{34,72} D. Buskulic,⁷ C. Buy,³⁵ R. L. Byer,⁴⁷ M. Cabero,⁹ L. Cadonati,⁷³ G. Cagnoli,^{25,74} C. Cahillane,¹ J. Calderón Bustillo,⁷³ T. A. Callister,¹ E. Calloni,^{75,4} J. B. Camp,⁷⁶ M. Canepa,^{54,55} P. Canizares,⁶¹ K. C. Cannon,⁷⁷ H. Cao,⁷⁸ J. Cao,⁷⁹ C. D. Capano,⁹ E. Capocasa,³⁵ F. Carbognani,²⁸ S. Caride,⁸⁰ M. F. Carney,⁸¹ J. Casanueva Diaz,²⁶ C. Casentini,^{30,17} S. Caudill,²⁰ M. Cavaglià,¹⁰ F. Cavalier,²⁶ R. Cavalieri,²⁸ G. Cella,²³ C. B. Cepeda,¹ L. Cerboni Baiardi,^{65,66} G. Cerretani,^{22,23} E. Cesarin,^{30,17} S. J. Chamberlin,⁸² M. Chan,⁴³ S. Chao,⁸³ P. Charlton,⁸⁴ E. Chassande-Mottin,³⁵ D. Chatterjee,²⁰ K. Chatzioannou,⁸⁵ B. D. Cheeseboro,^{37,38} H. Y. Chen,⁸⁶ Y. Chen,⁵⁹ H.-P. Cheng,⁵ A. Chincarini,⁵⁵ A. Chiummo,²⁸ T. Chmiel,⁸¹ H. S. Cho,⁸⁷ M. Cho,⁷² J. H. Chow,²⁴ N. Christensen,^{69,62} Q. Chu,⁶⁰ A. J. K. Chua,¹² S. Chua,⁶⁸ A. K. W. Chung,⁸⁸ S. Chung,⁶⁰ G. Ciani,⁵ R. Ciolfi,^{89,90} C. E. Cirelli,⁴⁷ A. Cirone,^{54,55} F. Clara,⁴⁴ J. A. Clark,⁷³ F. Cleva,⁶² C. Cocchieri,¹⁰ E. Coccia,^{16,17} P.-F. Cohadon,⁶⁸ A. Colla,^{91,32} C. G. Collette,⁹² L. R. Cominsky,⁹³ M. Constancio Jr.,¹⁵ L. Conti,⁵⁰ S. J. Cooper,⁵³ P. Corban,⁶ T. R. Corbitt,² K. R. Corley,⁴⁶ N. Cornish,⁹⁴ A. Corsi,⁸⁰ S. Cortese,²⁸ C. A. Costa,¹⁵ M. W. Coughlin,⁶⁹ S. B. Coughlin,^{95,96} J.-P. Coulon,⁶² S. T. Countryman,⁴⁶ P. Couvares,¹ P. B. Covas,⁹⁷ E. E. Cowan,⁷³ D. M. Coward,⁶⁰ M. J. Cowart,⁶ D. C. Coyne,¹ R. Coyne,⁸⁰ J. D. E. Creighton,²⁰ T. D. Creighton,⁹⁸ J. Cripe,² S. G. Crowder,⁹⁹ T. J. Cullen,²⁷ A. Cumming,⁴³ L. Cunningham,⁴³ E. Cuoco,²⁸ T. Dal Canton,⁷⁶ S. L. Danilishin,^{21,9} S. D'Antonio,¹⁷ K. Danzmann,^{21,9} A. Dasgupta,¹⁰⁰ C. F. Da Silva Costa,⁵ V. Dattilo,²⁸ I. Dave,⁵⁶ M. Davier,²⁶ D. Davis,⁴¹ E. J. Daw,¹⁰¹ B. Day,⁷³ S. De,⁴¹ D. DeBra,⁴⁷ E. Deelman,¹⁰² J. Degallaix,²⁵ M. De Laurentis,^{75,4} S. Deléglise,⁶⁸ W. Del Pozzo,^{53,22,23} T. Denker,⁹ T. Dent,⁹ V. Dergachev,³⁴ R. De Rosa,^{75,4} R. T. DeRosa,⁶ R. DeSalvo,¹⁰³ J. Devenson,⁵⁸ R. C. Devine,^{37,38} S. Dhurandhar,¹⁸ M. C. Díaz,⁹⁸ L. Di Fiore,⁴ M. Di Giovanni,^{104,90} T. Di Girolamo,^{75,4,46} A. Di Lieto,^{22,23} S. Di Pace,^{91,32} I. Di Palma,^{91,32} F. Di Renzo,^{22,23} Z. Doctor,⁸⁶ V. Dolique,²⁵ F. Donovan,¹⁴ K. L. Dooley,¹⁰ S. Doravari,⁹ I. Dorrington,⁹⁶ R. Douglas,⁴³ M. Dovale Álvarez,⁵³ T. P. Downes,²⁰ M. Drago,⁹ R. W. P. Drever†,¹ J. C. Driggers,⁴⁴ Z. Du,⁷⁹ M. Ducrot,⁷ J. Duncan,⁹⁵ S. E. Dwyer,⁴⁴ T. B. Edo,¹⁰¹ M. C. Edwards,⁶⁹ A. Effler,⁶ H.-B. Eggenstein,⁹ P. Ehrens,¹ J. Eichholz,¹ S. S. Eikenberry,⁵ R. A. Eisenstein,¹⁴ R. C. Essick,¹⁴ Z. B. Etienne,^{37,38} T. Etzel,¹ M. Evans,¹⁴ T. M. Evans,⁶ M. Factourovich,⁴⁶ V. Fafone,^{30,17,16} H. Fair,⁴¹ S. Fairhurst,⁹⁶ X. Fan,⁷⁹ S. Farinon,⁵⁵ B. Farr,⁸⁶ W. M. Farr,⁵³ E. J. Fauchon-Jones,⁹⁶ M. Favata,¹⁰⁵ M. Fays,⁹⁶ H. Fehrmann,⁹ J. Feicht,¹ M. M. Fejer,⁴⁷ A. Fernandez-Galiana,¹⁴ I. Ferrante,^{22,23} E. C. Ferreira,¹⁵ F. Ferrini,²⁸ F. Fidecaro,^{22,23} I. Fiori,²⁸ D. Fiorucci,³⁵ R. P. Fisher,⁴¹ R. Flaminio,^{25,106} M. Fletcher,⁴³ H. Fong,⁸⁵ P. W. F. Forsyth,²⁴ S. S. Forsyth,⁷³ J.-D. Fournier,⁶² S. Frasca,^{91,32} F. Frasconi,²³ Z. Frei,⁵¹ A. Freise,⁵³ R. Frey,⁶⁷ V. Frey,²⁶ E. M. Fries,¹ P. Fritschel,¹⁴ V. V. Frolov,⁶ P. Fulda,^{5,76} M. Fyffe,⁶ H. Gabbard,⁹ M. Gabel,¹⁰⁷ B. U. Gadre,¹⁸ S. M. Gaebel,⁵³ J. R. Gair,¹⁰⁸ L. Gammaitoni,³⁹ M. R. Ganija,⁷⁸ S. G. Gaonkar,¹⁸ F. Garufi,^{75,4} S. Gaudio,³³ G. Gaur,¹⁰⁹ V. Gayathri,¹¹⁰ N. Gehrels†,⁷⁶ G. Gemme,⁵⁵ E. Genin,²⁸ A. Gennai,²³ D. George,¹¹ J. George,⁵⁶ L. Gergely,¹¹¹ V. Germain,⁷ S. Ghonge,⁷³ Abhirup Ghosh,¹⁹ Archisman Ghosh,^{19,13} S. Ghosh,^{61,13} J. A. Giaime,^{2,6} K. D. Giardina,⁶ A. Giazotto,²³ K. Gill,³³ L. Glover,¹⁰³ E. Goetz,⁹ R. Goetz,⁵ S. Gomes,⁹⁶ G. González,² J. M. Gonzalez Castro,^{22,23} A. Gopakumar,¹¹² M. L. Gorodetsky,⁵⁷ S. E. Gossan,¹ M. Gosselin,²⁸ R. Gouaty,⁷ A. Grado,^{113,4} C. Graef,⁴³ M. Granata,²⁵

- A. Grant,⁴³ S. Gras,¹⁴ C. Gray,⁴⁴ G. Greco,^{65,66} A. C. Green,⁵³ P. Groot,⁶¹ H. Grote,⁹ S. Grunewald,³⁴
 P. Gruning,²⁶ G. M. Guidi,^{65,66} X. Guo,⁷⁹ A. Gupta,⁸² M. K. Gupta,¹⁰⁰ K. E. Gushwa,¹ E. K. Gustafson,¹
 R. Gustafson,¹¹⁴ B. R. Hall,⁶⁴ E. D. Hall,¹ G. Hammond,⁴³ M. Haney,¹¹² M. M. Hanke,⁹ J. Hanks,⁴⁴ C. Hanna,⁸²
 M. D. Hannam,⁹⁶ O. A. Hannuksela,⁸⁸ J. Hanson,⁶ T. Hardwick,² J. Harms,^{65,66} G. M. Harry,¹¹⁵ I. W. Harry,³⁴
 M. J. Hart,⁴³ C.-J. Haster,⁸⁵ K. Haughian,⁴³ J. Healy,¹¹⁶ A. Heidmann,⁶⁸ M. C. Heintze,⁶ H. Heitmann,⁶²
 P. Hello,²⁶ G. Hemming,²⁸ M. Hendry,⁴³ I. S. Heng,⁴³ J. Hennig,⁴³ J. Henry,¹¹⁶ A. W. Heptonstall,¹ M. Heurs,^{9,21}
 S. Hild,⁴³ D. Hoak,²⁸ D. Hofman,²⁵ K. Holt,⁶ D. E. Holz,⁸⁶ P. Hopkins,⁹⁶ C. Horst,²⁰ J. Hough,⁴³ E. A. Houston,⁴³
 E. J. Howell,⁶⁰ Y. M. Hu,⁹ E. A. Huerta,¹¹ D. Huet,²⁶ B. Hughey,³³ S. Husa,⁹⁷ S. H. Huttner,⁴³ T. Huynh-Dinh,⁶
 N. Indik,⁹ D. R. Ingram,⁴⁴ R. Inta,⁸⁰ G. Intini,^{91,32} H. N. Isa,⁴³ J.-M. Isac,⁶⁸ M. Isi,¹ B. R. Iyer,¹⁹ K. Izumi,⁴⁴
 T. Jacqmin,⁶⁸ K. Jani,⁷³ P. Jaranowski,¹¹⁷ S. Jawahar,¹¹⁸ F. Jiménez-Forteza,⁹⁷ W. W. Johnson,²
 N. K. Johnson-McDaniel,¹⁹ D. I. Jones,¹¹⁹ R. Jones,⁴³ R. J. G. Jonker,¹³ L. Ju,⁶⁰ J. Junker,⁹ C. V. Kalaghatgi,⁹⁶
 V. Kalogera,⁹⁵ S. Kandhasamy,⁶ G. Kang,³⁶ J. B. Kanner,¹ S. Karki,⁶⁷ K. S. Karvinen,⁹ M. Kasprzack,²
 M. Katolik,¹¹ E. Katsavounidis,¹⁴ W. Katzman,⁶ S. Kaufer,²¹ K. Kawabe,⁴⁴ F. Kéfélian,⁶² D. Keitel,⁴³
 A. J. Kemball,¹¹ R. Kennedy,¹⁰¹ C. Kent,⁹⁶ J. S. Key,¹²⁰ F. Y. Khalili,⁵⁷ I. Khan,^{16,17} S. Khan,⁹ Z. Khan,¹⁰⁰
 E. A. Khazanov,¹²¹ N. Kijbunchoo,⁴⁴ Chunglee Kim,¹²² J. C. Kim,¹²³ W. Kim,⁷⁸ W. S. Kim,¹²⁴ Y.-M. Kim,^{87,122}
 S. J. Kimbrell,⁷³ E. J. King,⁷⁸ P. J. King,⁴⁴ R. Kirchhoff,⁹ J. S. Kissel,⁴⁴ L. Kleybolte,³¹ S. Klimenko,⁵ P. Koch,⁹
 S. M. Koehlenbeck,⁹ S. Koley,¹³ V. Kondrashov,¹ A. Kontos,¹⁴ M. Korobko,³¹ W. Z. Korth,¹ I. Kowalska,⁷⁰
 D. B. Kozak,¹ C. Krämer,⁹ V. Kringel,⁹ B. Krishnan,⁹ A. Królak,^{125,126} G. Kuehn,⁹ P. Kumar,⁸⁵ R. Kumar,¹⁰⁰
 S. Kumar,¹⁹ L. Kuo,⁸³ A. Kutynia,¹²⁵ S. Kwang,²⁰ B. D. Lackey,³⁴ K. H. Lai,⁸⁸ M. Landry,⁴⁴ R. N. Lang,²⁰
 J. Lange,¹¹⁶ B. Lantz,⁴⁷ R. K. Lanza,¹⁴ A. Lartaux-Vollard,²⁶ P. D. Lasky,¹²⁷ M. Laxen,⁶ A. Lazzarini,¹
 C. Lazzaro,⁵⁰ P. Leaci,^{91,32} S. Leavey,⁴³ C. H. Lee,⁸⁷ H. K. Lee,¹²⁸ H. M. Lee,¹²² H. W. Lee,¹²³ K. Lee,⁴³
 J. Lehmann,⁹ A. Lenon,^{37,38} M. Leonardi,^{104,90} N. Leroy,²⁶ N. Letendre,⁷ Y. Levin,¹²⁷ T. G. F. Li,⁸⁸
 A. Libson,¹⁴ T. B. Littenberg,¹²⁹ J. Liu,⁶⁰ R. K. L. Lo,⁸⁸ N. A. Lockerbie,¹¹⁸ L. T. London,⁹⁶ J. E. Lord,⁴¹
 M. Lorenzini,^{16,17} V. Loriette,¹³⁰ M. Lormand,⁶ G. Losurdo,²³ J. D. Lough,^{9,21} G. Lovelace,²⁷ H. Lück,^{21,9}
 D. Lumaca,^{30,17} A. P. Lundgren,⁹ R. Lynch,¹⁴ Y. Ma,⁵⁹ S. Macfoy,⁵⁸ B. Machenschalk,⁹ M. MacInnis,¹⁴
 D. M. Macleod,² I. Magaña Hernandez,⁸⁸ F. Magaña-Sandoval,⁴¹ L. Magaña Zertuche,⁴¹ R. M. Magee,⁸²
 E. Majorana,³² I. Maksimovic,¹³⁰ N. Man,⁶² V. Mandic,⁴² V. Mangano,⁴³ G. L. Mansell,²⁴ M. Manske,²⁰
 M. Mantovani,²⁸ F. Marchesoni,^{48,40} F. Marion,⁷ S. Márka,⁴⁶ Z. Márka,⁴⁶ C. Markakis,¹¹ A. S. Markosyan,⁴⁷
 E. Maros,¹ F. Martelli,^{65,66} L. Martellini,⁶² I. W. Martin,⁴³ D. V. Martynov,¹⁴ J. N. Marx,¹ K. Mason,¹⁴
 A. Masserot,⁷ T. J. Massinger,¹ M. Masso-Reid,⁴³ S. Mastrogiovanni,^{91,32} A. Matas,⁴² F. Matichard,¹⁴ L. Matone,⁴⁶
 N. Mavalvala,¹⁴ R. Mayani,¹⁰² N. Mazumder,⁶⁴ R. McCarthy,⁴⁴ D. E. McClelland,²⁴ S. McCormick,⁶ L. McCuller,¹⁴
 S. C. McGuire,¹³¹ G. McIntyre,¹ J. McIver,¹ D. J. McManus,²⁴ T. McRae,²⁴ S. T. McWilliams,^{37,38} D. Meacher,⁸²
 G. D. Meadors,^{34,9} J. Meidam,¹³ E. Mejuto-Villa,⁸ A. Melatos,¹³² G. Mendell,⁴⁴ R. A. Mercer,²⁰ E. L. Merilh,⁴⁴
 M. Merzougui,⁶² S. Meshkov,¹ C. Messenger,⁴³ C. Messick,⁸² R. Metzdorff,⁶⁸ P. M. Meyers,⁴² F. Mezzani,^{32,91}
 H. Miao,⁵³ C. Michel,²⁵ H. Middleton,⁵³ E. E. Mikhailov,¹³³ L. Milano,^{75,4} A. L. Miller,⁵ A. Miller,^{91,32}
 B. B. Miller,⁹⁵ J. Miller,¹⁴ M. Millhouse,⁹⁴ O. Minazzoli,⁶² Y. Minenkov,¹⁷ J. Ming,³⁴ C. Mishra,¹³⁴ S. Mitra,¹⁸
 V. P. Mitrofanov,⁵⁷ G. Mitselmakher,⁵ R. Middleman,¹⁴ A. Moggi,²³ M. Mohan,²⁸ S. R. P. Mohapatra,¹⁴
 M. Montani,^{65,66} B. C. Moore,¹⁰⁵ C. J. Moore,¹² D. Moraru,⁴⁴ G. Moreno,⁴⁴ S. R. Morris,⁹⁸ B. Mouris,⁷
 C. M. Mow-Lowry,⁵³ G. Mueller,⁵ A. W. Muir,⁹⁶ Arunava Mukherjee,⁹ D. Mukherjee,²⁰ S. Mukherjee,⁹⁸
 N. Mukund,¹⁸ A. Mullavey,⁶ J. Munch,⁷⁸ E. A. M. Muniz,⁴¹ P. G. Murray,⁴³ K. Napier,⁷³ I. Nardecchia,^{30,17}
 L. Naticchioni,^{91,32} R. K. Nayak,¹³⁵ G. Nelemans,^{61,13} T. J. N. Nelson,⁶ M. Neri,^{54,55} M. Nery,⁹ A. Neunzert,¹¹⁴
 J. M. Newport,¹¹⁵ G. Newton^{‡,43} K. K. Y. Ng,⁸⁸ T. T. Nguyen,²⁴ D. Nichols,⁶¹ A. B. Nielsen,⁹ S. Nissanke,^{61,13}
 A. Nitz,⁹ A. Noack,⁹ F. Nocera,²⁸ D. Nolting,⁶ M. E. N. Normandin,⁹⁸ L. K. Nuttall,⁴¹ J. Oberling,⁴⁴ E. Ochsner,²⁰
 E. Oelker,¹⁴ G. H. Ogin,¹⁰⁷ J. J. Oh,¹²⁴ S. H. Oh,¹²⁴ F. Ohme,⁹ M. Oliver,⁹⁷ P. Oppermann,⁹ Richard J. Oram,⁶
 B. O'Reilly,⁶ R. Ormiston,⁴² L. F. Ortega,⁵ R. O'Shaughnessy,¹¹⁶ D. J. Ottaway,⁷⁸ H. Overmier,⁶ B. J. Owen,⁸⁰
 A. E. Pace,⁸² J. Page,¹²⁹ M. A. Page,⁶⁰ A. Pai,¹¹⁰ S. A. Pai,⁵⁶ J. R. Palamos,⁶⁷ O. Palashov,¹²¹ C. Palomba,³²
 A. Pal-Singh,³¹ H. Pan,⁸³ B. Pang,⁵⁹ P. T. H. Pang,⁸⁸ C. Pankow,⁹⁵ F. Pannarale,⁹⁶ B. C. Pant,⁵⁶ F. Paoletti,²³
 A. Paoli,²⁸ M. A. Papa,^{34,20,9} H. R. Paris,⁴⁷ W. Parker,⁶ D. Pascucci,⁴³ A. Pasqualetti,²⁸ R. Passaquieti,^{22,23}
 D. Passuello,²³ B. Patricelli,^{136,23} B. L. Pearlstone,⁴³ M. Pedraza,¹ R. Pedurand,^{25,137} L. Pekowsky,⁴¹ A. Pele,⁶
 S. Penn,¹³⁸ C. J. Perez,⁴⁴ A. Perreca,^{1,104,90} L. M. Perri,⁹⁵ H. P. Pfeiffer,⁸⁵ M. Phelps,⁴³ O. J. Piccinni,^{91,32}
 M. Pichot,⁶² F. Piergiovanni,^{65,66} V. Pierro,⁸ G. Pillant,²⁸ L. Pinard,²⁵ I. M. Pinto,⁸ M. Pitkin,⁴³ R. Poggiani,^{22,23}
 P. Popolizio,²⁸ E. K. Porter,³⁵ A. Post,⁹ J. Powell,⁴³ J. Prasad,¹⁸ J. W. W. Pratt,³³ V. Predoi,⁹⁶ T. Prestegard,²⁰
 M. Prijatelj,⁹ M. Principe,⁸ S. Privitera,³⁴ G. A. Prodi,^{104,90} L. G. Prokhorov,⁵⁷ O. Puncken,⁹ M. Punturo,⁴⁰

- P. Puppo,³² M. Pürller,³⁴ H. Qi,²⁰ J. Qin,⁶⁰ S. Qiu,¹²⁷ V. Quetschke,⁹⁸ E. A. Quintero,¹ R. Quitzow-James,⁶⁷
 F. J. Raab,⁴⁴ D. S. Rabeling,²⁴ H. Radkins,⁴⁴ P. Raffai,⁵¹ S. Raja,⁵⁶ C. Rajan,⁵⁶ M. Rakhmanov,⁹⁸
 K. E. Ramirez,⁹⁸ P. Rapagnani,^{91,32} V. Raymond,³⁴ M. Razzano,^{22,23} J. Read,²⁷ T. Regimbau,⁶² L. Rei,⁵⁵
 S. Reid,⁵⁸ D. H. Reitze,^{1,5} H. Rew,¹³³ S. D. Reyes,⁴¹ F. Ricci,^{91,32} P. M. Ricker,¹¹ S. Rieger,⁹ K. Riles,¹¹⁴
 M. Rizzo,¹¹⁶ N. A. Robertson,^{1,43} R. Robie,⁴³ F. Robinet,²⁶ A. Rocchi,¹⁷ L. Rolland,⁷ J. G. Rollins,¹ V. J. Roma,⁶⁷
 J. D. Romano,⁹⁸ R. Romano,^{3,4} C. L. Romel,⁴⁴ J. H. Romie,⁶ D. Rosińska,^{139,52} M. P. Ross,¹⁴⁰ S. Rowan,⁴³
 A. Rüdiger,⁹ P. Ruggi,²⁸ K. Ryan,⁴⁴ M. Rynge,¹⁰² S. Sachdev,¹ T. Sadecki,⁴⁴ L. Sadeghian,²⁰ M. Sakellariadou,¹⁴¹
 L. Salconi,²⁸ M. Saleem,¹¹⁰ F. Salemi,⁹ A. Samajdar,¹³⁵ L. Sammut,¹²⁷ L. M. Sampson,⁹⁵ E. J. Sanchez,¹
 V. Sandberg,⁴⁴ B. Sandeen,⁹⁵ J. R. Sanders,⁴¹ B. Sassolas,²⁵ B. S. Sathyaprakash,^{82,96} P. R. Saulson,⁴¹
 O. Sauter,¹¹⁴ R. L. Savage,⁴⁴ A. Sawadsky,²¹ P. Schale,⁶⁷ J. Scheuer,⁹⁵ E. Schmidt,³³ J. Schmidt,⁹ P. Schmidt,^{1,61}
 R. Schnabel,³¹ R. M. S. Schofield,⁶⁷ A. Schönbeck,³¹ E. Schreiber,⁹ D. Schuette,^{9,21} B. W. Schulte,⁹
 B. F. Schutz,^{96,9} S. G. Schwalbe,³³ J. Scott,⁴³ S. M. Scott,²⁴ E. Seidel,¹¹ D. Sellers,⁶ A. S. Sengupta,¹⁴²
 D. Sentenac,²⁸ V. Sequino,^{30,17} A. Sergeev,¹²¹ D. A. Shaddock,²⁴ T. J. Shaffer,⁴⁴ A. A. Shah,¹²⁹ M. S. Shahriar,⁹⁵
 L. Shao,³⁴ B. Shapiro,⁴⁷ P. Shawhan,⁷² A. Sheperd,²⁰ D. H. Shoemaker,¹⁴ D. M. Shoemaker,⁷³ K. Siellez,⁷³
 X. Siemens,²⁰ M. Sieniawska,⁵² D. Sigg,⁴⁴ A. D. Silva,¹⁵ A. Singer,¹ L. P. Singer,⁷⁶ A. Singh,^{34,9,21} R. Singh,²
 A. Singhal,^{16,32} A. M. Sintes,⁹⁷ B. J. J. Slagmolen,²⁴ B. Smith,⁶ J. R. Smith,²⁷ R. J. E. Smith,¹ E. J. Son,¹²⁴
 J. A. Sonnenberg,²⁰ B. Sorazu,⁴³ F. Sorrentino,⁵⁵ T. Souradeep,¹⁸ A. P. Spencer,⁴³ A. K. Srivastava,¹⁰⁰ A. Staley,⁴⁶
 M. Steinke,⁹ J. Steinlechner,^{43,31} S. Steinlechner,³¹ D. Steinmeyer,^{9,21} B. C. Stephens,²⁰ S. P. Stevenson,⁵³
 R. Stone,⁹⁸ K. A. Strain,⁴³ G. Stratta,^{65,66} S. E. Strigin,⁵⁷ R. Sturani,¹⁴³ A. L. Stuver,⁶ T. Z. Summerscales,¹⁴⁴
 L. Sun,¹³² S. Sunil,¹⁰⁰ P. J. Sutton,⁹⁶ B. L. Swinkels,²⁸ M. J. Szczepańczyk,³³ M. Tacca,³⁵ D. Talukder,⁶⁷
 D. B. Tanner,⁵ M. Tápai,¹¹¹ A. Taracchini,³⁴ J. A. Taylor,¹²⁹ R. Taylor,¹ T. Theeg,⁹ E. G. Thomas,⁵³ M. Thomas,⁶
 P. Thomas,⁴⁴ K. A. Thorne,⁶ K. S. Thorne,⁵⁹ E. Thrane,¹²⁷ S. Tiwari,^{16,90} V. Tiwari,⁹⁶ K. V. Tokmakov,¹¹⁸
 K. Toland,⁴³ M. Tonelli,^{22,23} Z. Tornasi,⁴³ C. I. Torrie,¹ D. Töyrä,⁵³ F. Travasso,^{28,40} G. Traylor,⁶ D. Trifirò,¹⁰
 J. Trinastic,⁵ M. C. Tringali,^{104,90} L. Trozzo,^{145,23} K. W. Tsang,¹³ M. Tse,¹⁴ R. Tso,¹ D. Tuyenbayev,⁹⁸
 K. Ueno,²⁰ D. Ugolini,¹⁴⁶ C. S. Unnikrishnan,¹¹² A. L. Urban,¹ S. A. Usman,⁹⁶ K. Vahi,¹⁰² H. Vahlbruch,²¹
 G. Vajente,¹ G. Valdes,⁹⁸ M. Vallisneri,⁵⁹ N. van Bakel,¹³ M. van Beuzekom,¹³ J. F. J. van den Brand,^{71,13}
 C. Van Den Broeck,¹³ D. C. Vander-Hyde,⁴¹ L. van der Schaaf,¹³ J. V. van Heijningen,¹³ A. A. van Veggel,⁴³
 M. Vardaro,^{49,50} V. Varma,⁵⁹ S. Vass,¹ M. Vasúth,⁴⁵ A. Vecchio,⁵³ G. Vedovato,⁵⁰ J. Veitch,⁵³ P. J. Veitch,⁷⁸
 K. Venkateswara,¹⁴⁰ G. Venugopalan,¹ D. Verkindt,⁷ F. Vetrano,^{65,66} A. Viceré,^{65,66} A. D. Viets,²⁰ S. Vinciguerra,⁵³
 D. J. Vine,⁵⁸ J.-Y. Vinet,⁶² S. Vitale,¹⁴ T. Vo,⁴¹ H. Vocca,^{39,40} C. Vorvick,⁴⁴ D. V. Voss,⁵ W. D. Vousden,⁵³
 S. P. Vyatchanin,⁵⁷ A. R. Wade,¹ L. E. Wade,⁸¹ M. Wade,⁸¹ R. M. Wald,⁸⁶ R. Walet,¹³ M. Walker,² L. Wallace,¹
 S. Walsh,²⁰ G. Wang,^{16,66} H. Wang,⁵³ J. Z. Wang,⁸² M. Wang,⁵³ Y.-F. Wang,⁸⁸ Y. Wang,⁶⁰ R. L. Ward,²⁴
 J. Warner,⁴⁴ M. Was,⁷ J. Watchi,⁹² B. Weaver,⁴⁴ L.-W. Wei,^{9,21} M. Weinert,⁹ A. J. Weinstein,¹ R. Weiss,¹⁴
 L. Wen,⁶⁰ E. K. Wessel,¹¹ P. Weßels,⁹ T. Westphal,⁹ K. Wette,⁹ J. T. Whelan,¹¹⁶ B. F. Whiting,⁵ C. Whittle,¹²⁷
 D. Williams,⁴³ R. D. Williams,¹ A. R. Williamson,¹¹⁶ J. L. Willis,¹⁴⁷ B. Willke,^{21,9} M. H. Wimmer,^{9,21} W. Winkler,⁹
 C. C. Wipf,¹ H. Wittel,^{9,21} G. Woan,⁴³ J. Woehler,⁹ J. Wofford,¹¹⁶ K. W. K. Wong,⁸⁸ J. Worden,⁴⁴ J. L. Wright,⁴³
 D. S. Wu,⁹ G. Wu,⁶ W. Yam,¹⁴ H. Yamamoto,¹ C. C. Yancey,⁷² M. J. Yap,²⁴ Hang Yu,¹⁴ Haocun Yu,¹⁴ M. Yvert,⁷
 A. Zadrożny,¹²⁵ M. Zanolini,³³ T. Zelenova,²⁸ J.-P. Zendri,⁵⁰ M. Zevin,⁹⁵ L. Zhang,¹ M. Zhang,¹³³ T. Zhang,⁴³
 Y.-H. Zhang,¹¹⁶ C. Zhao,⁶⁰ M. Zhou,⁹⁵ Z. Zhou,⁹⁵ X. J. Zhu,⁶⁰ A. Zimmerman,⁸⁵ M. E. Zucker,^{1,14} and J. Zweizig¹

(LIGO Scientific Collaboration and Virgo Collaboration)

^{*}Deceased, March 2016. [#]Deceased, March 2017. [†]Deceased, February 2017. [‡]Deceased, December 2016.¹LIGO, California Institute of Technology, Pasadena, CA 91125, USA²Louisiana State University, Baton Rouge, LA 70803, USA³Università di Salerno, Fisciano, I-84084 Salerno, Italy⁴INFN, Sezione di Napoli, Complesso Universitario di Monte S. Angelo, I-80126 Napoli, Italy⁵University of Florida, Gainesville, FL 32611, USA⁶LIGO Livingston Observatory, Livingston, LA 70754, USA⁷Laboratoire d'Annecy-le-Vieux de Physique des Particules (LAPP),

Université Savoie Mont Blanc, CNRS/IN2P3, F-74941 Annecy, France

⁸University of Sannio at Benevento, I-82100 Benevento,

Italy and INFN, Sezione di Napoli, I-80100 Napoli, Italy

⁹Albert-Einstein-Institut, Max-Planck-Institut für Gravitationsphysik, D-30167 Hannover, Germany¹⁰The University of Mississippi, University, MS 38677, USA¹¹NCSA, University of Illinois at Urbana-Champaign, Urbana, IL 61801, USA¹²University of Cambridge, Cambridge CB2 1TN, United Kingdom

- ¹³Nikhef, Science Park, 1098 XG Amsterdam, Netherlands
¹⁴LIGO, Massachusetts Institute of Technology, Cambridge, MA 02139, USA
¹⁵Instituto Nacional de Pesquisas Espaciais, 12227-010 São José dos Campos, São Paulo, Brazil
¹⁶Gran Sasso Science Institute (GSSI), I-67100 L’Aquila, Italy
¹⁷INFN, Sezione di Roma Tor Vergata, I-00133 Roma, Italy
¹⁸Inter-University Centre for Astronomy and Astrophysics, Pune 411007, India
¹⁹International Centre for Theoretical Sciences, Tata Institute of Fundamental Research, Bengaluru 560089, India
²⁰University of Wisconsin-Milwaukee, Milwaukee, WI 53201, USA
²¹Leibniz Universität Hannover, D-30167 Hannover, Germany
²²Università di Pisa, I-56127 Pisa, Italy
²³INFN, Sezione di Pisa, I-56127 Pisa, Italy
²⁴OzGrav, Australian National University, Canberra, Australian Capital Territory 0200, Australia
²⁵Laboratoire des Matériaux Avancés (LMA), CNRS/IN2P3, F-69622 Villeurbanne, France
²⁶LAL, Univ. Paris-Sud, CNRS/IN2P3, Université Paris-Saclay, F-91898 Orsay, France
²⁷California State University Fullerton, Fullerton, CA 92831, USA
²⁸European Gravitational Observatory (EGO), I-56021 Cascina, Pisa, Italy
²⁹Chennai Mathematical Institute, Chennai 603103, India
³⁰Università di Roma Tor Vergata, I-00133 Roma, Italy
³¹Universität Hamburg, D-22761 Hamburg, Germany
³²INFN, Sezione di Roma, I-00185 Roma, Italy
³³Embry-Riddle Aeronautical University, Prescott, AZ 86301, USA
³⁴Albert-Einstein-Institut, Max-Planck-Institut für Gravitationsphysik, D-14476 Potsdam-Golm, Germany
³⁵APC, AstroParticule et Cosmologie, Université Paris Diderot,
CNRS/IN2P3, CEA/Irfu, Observatoire de Paris,
Sorbonne Paris Cité, F-75205 Paris Cedex 13, France
³⁶Korea Institute of Science and Technology Information, Daejeon 34141, Korea
³⁷West Virginia University, Morgantown, WV 26506, USA
³⁸Center for Gravitational Waves and Cosmology,
West Virginia University, Morgantown, WV 26505, USA
³⁹Università di Perugia, I-06123 Perugia, Italy
⁴⁰INFN, Sezione di Perugia, I-06123 Perugia, Italy
⁴¹Syracuse University, Syracuse, NY 13244, USA
⁴²University of Minnesota, Minneapolis, MN 55455, USA
⁴³SUPA, University of Glasgow, Glasgow G12 8QQ, United Kingdom
⁴⁴LIGO Hanford Observatory, Richland, WA 99352, USA
⁴⁵Wigner RCP, RMKI, H-1121 Budapest, Konkoly Thege Miklós út 29-33, Hungary
⁴⁶Columbia University, New York, NY 10027, USA
⁴⁷Stanford University, Stanford, CA 94305, USA
⁴⁸Università di Camerino, Dipartimento di Fisica, I-62032 Camerino, Italy
⁴⁹Università di Padova, Dipartimento di Fisica e Astronomia, I-35131 Padova, Italy
⁵⁰INFN, Sezione di Padova, I-35131 Padova, Italy
⁵¹MTA Eötvös University, “Lendulet” Astrophysics Research Group, Budapest 1117, Hungary
⁵²Nicolaus Copernicus Astronomical Center, Polish Academy of Sciences, 00-716, Warsaw, Poland
⁵³University of Birmingham, Birmingham B15 2TT, United Kingdom
⁵⁴Università degli Studi di Genova, I-16146 Genova, Italy
⁵⁵INFN, Sezione di Genova, I-16146 Genova, Italy
⁵⁶RRCAT, Indore MP 452013, India
⁵⁷Faculty of Physics, Lomonosov Moscow State University, Moscow 119991, Russia
⁵⁸SUPA, University of the West of Scotland, Paisley PA1 2BE, United Kingdom
⁵⁹Caltech CaRT, Pasadena, CA 91125, USA
⁶⁰OzGrav, University of Western Australia, Crawley, Western Australia 6009, Australia
⁶¹Department of Astrophysics/IMAPP, Radboud University Nijmegen,
P.O. Box 9010, 6500 GL Nijmegen, Netherlands
⁶²Artemis, Université Côte d’Azur, Observatoire Côte d’Azur,
CNRS, CS 34229, F-06304 Nice Cedex 4, France
⁶³Institut de Physique de Rennes, CNRS, Université de Rennes 1, F-35042 Rennes, France
⁶⁴Washington State University, Pullman, WA 99164, USA
⁶⁵Università degli Studi di Urbino “Carlo Bo”, I-61029 Urbino, Italy
⁶⁶INFN, Sezione di Firenze, I-50019 Sesto Fiorentino, Firenze, Italy
⁶⁷University of Oregon, Eugene, OR 97403, USA
⁶⁸Laboratoire Kastler Brossel, UPMC-Sorbonne Universités, CNRS,
ENS-PSL Research University, Collège de France, F-75005 Paris, France
⁶⁹Carleton College, Northfield, MN 55057, USA
⁷⁰Astronomical Observatory Warsaw University, 00-478 Warsaw, Poland

- ⁷¹ VU University Amsterdam, 1081 HV Amsterdam, Netherlands
⁷² University of Maryland, College Park, MD 20742, USA
⁷³ Center for Relativistic Astrophysics and School of Physics,
 Georgia Institute of Technology, Atlanta, GA 30332, USA
⁷⁴ Université Claude Bernard Lyon 1, F-69622 Villeurbanne, France
⁷⁵ Università di Napoli “Federico II”, Complesso Universitario di Monte S. Angelo, I-80126 Napoli, Italy
⁷⁶ NASA Goddard Space Flight Center, Greenbelt, MD 20771, USA
⁷⁷ RESCEU, University of Tokyo, Tokyo, 113-0033, Japan
⁷⁸ OzGrav, University of Adelaide, Adelaide, South Australia 5005, Australia
⁷⁹ Tsinghua University, Beijing 100084, China
⁸⁰ Texas Tech University, Lubbock, TX 79409, USA
⁸¹ Kenyon College, Gambier, OH 43022, USA
⁸² The Pennsylvania State University, University Park, PA 16802, USA
⁸³ National Tsing Hua University, Hsinchu City, 30013 Taiwan, Republic of China
⁸⁴ Charles Sturt University, Wagga Wagga, New South Wales 2678, Australia
⁸⁵ Canadian Institute for Theoretical Astrophysics,
 University of Toronto, Toronto, Ontario M5S 3H8, Canada
⁸⁶ University of Chicago, Chicago, IL 60637, USA
⁸⁷ Pusan National University, Busan 46241, Korea
⁸⁸ The Chinese University of Hong Kong, Shatin, NT, Hong Kong
⁸⁹ INAF, Osservatorio Astronomico di Padova, Vicolo dell’Osservatorio 5, I-35122 Padova, Italy
⁹⁰ INFN, Trento Institute for Fundamental Physics and Applications, I-38123 Povo, Trento, Italy
⁹¹ Università di Roma “La Sapienza”, I-00185 Roma, Italy
⁹² Université Libre de Bruxelles, Brussels 1050, Belgium
⁹³ Sonoma State University, Rohnert Park, CA 94928, USA
⁹⁴ Montana State University, Bozeman, MT 59717, USA
⁹⁵ Center for Interdisciplinary Exploration & Research in Astrophysics (CIERA),
 Northwestern University, Evanston, IL 60208, USA
⁹⁶ Cardiff University, Cardiff CF24 3AA, United Kingdom
⁹⁷ Universitat de les Illes Balears, IAC3—IEEC, E-07122 Palma de Mallorca, Spain
⁹⁸ The University of Texas Rio Grande Valley, Brownsville, TX 78520, USA
⁹⁹ Bellevue College, Bellevue, WA 98007, USA
¹⁰⁰ Institute for Plasma Research, Bhat, Gandhinagar 382428, India
¹⁰¹ The University of Sheffield, Sheffield S10 2TN, United Kingdom
¹⁰² University of Southern California Information Sciences Institute, Marina Del Rey, CA 90292, USA
¹⁰³ California State University, Los Angeles, 5151 State University Dr, Los Angeles, CA 90032, USA
¹⁰⁴ Università di Trento, Dipartimento di Fisica, I-38123 Povo, Trento, Italy
¹⁰⁵ Montclair State University, Montclair, NJ 07043, USA
¹⁰⁶ National Astronomical Observatory of Japan, 2-21-1 Osawa, Mitaka, Tokyo 181-8588, Japan
¹⁰⁷ Whitman College, 345 Boyer Avenue, Walla Walla, WA 99362 USA
¹⁰⁸ School of Mathematics, University of Edinburgh, Edinburgh EH9 3FD, United Kingdom
¹⁰⁹ University and Institute of Advanced Research, Gandhinagar Gujarat 382007, India
¹¹⁰ IISER-TVM, CET Campus, Trivandrum Kerala 695016, India
¹¹¹ University of Szeged, Dóm tér 9, Szeged 6720, Hungary
¹¹² Tata Institute of Fundamental Research, Mumbai 400005, India
¹¹³ INAF, Osservatorio Astronomico di Capodimonte, I-80131, Napoli, Italy
¹¹⁴ University of Michigan, Ann Arbor, MI 48109, USA
¹¹⁵ American University, Washington, D.C. 20016, USA
¹¹⁶ Rochester Institute of Technology, Rochester, NY 14623, USA
¹¹⁷ University of Białystok, 15-424 Białystok, Poland
¹¹⁸ SUPA, University of Strathclyde, Glasgow G1 1XQ, United Kingdom
¹¹⁹ University of Southampton, Southampton SO17 1BJ, United Kingdom
¹²⁰ University of Washington Bothell, 18115 Campus Way NE, Bothell, WA 98011, USA
¹²¹ Institute of Applied Physics, Nizhny Novgorod, 603950, Russia
¹²² Seoul National University, Seoul 08826, Korea
¹²³ Inje University Gimhae, South Gyeongsang 50834, Korea
¹²⁴ National Institute for Mathematical Sciences, Daejeon 34047, Korea
¹²⁵ NCBJ, 05-400 Świerk-Otwock, Poland
¹²⁶ Institute of Mathematics, Polish Academy of Sciences, 00656 Warsaw, Poland
¹²⁷ OzGrav, School of Physics & Astronomy, Monash University, Clayton 3800, Victoria, Australia
¹²⁸ Hanyang University, Seoul 04763, Korea
¹²⁹ NASA Marshall Space Flight Center, Huntsville, AL 35811, USA
¹³⁰ ESPCI, CNRS, F-75005 Paris, France
¹³¹ Southern University and A&M College, Baton Rouge, LA 70813, USA

¹³²*OzGrav, University of Melbourne, Parkville, Victoria 3010, Australia*

¹³³*College of William and Mary, Williamsburg, VA 23187, USA*

¹³⁴*Indian Institute of Technology Madras, Chennai 600036, India*

¹³⁵*IISER-Kolkata, Mohanpur, West Bengal 741252, India*

¹³⁶*Scuola Normale Superiore, Piazza dei Cavalieri 7, I-56126 Pisa, Italy*

¹³⁷*Université de Lyon, F-69361 Lyon, France*

¹³⁸*Hobart and William Smith Colleges, Geneva, NY 14456, USA*

¹³⁹*Janusz Gil Institute of Astronomy, University of Zielona Góra, 65-265 Zielona Góra, Poland*

¹⁴⁰*University of Washington, Seattle, WA 98195, USA*

¹⁴¹*King’s College London, University of London, London WC2R 2LS, United Kingdom*

¹⁴²*Indian Institute of Technology, Gandhinagar Ahmedabad Gujarat 382424, India*

¹⁴³*International Institute of Physics, Universidade Federal do Rio Grande do Norte, Natal RN 59078-970, Brazil*

¹⁴⁴*Andrews University, Berrien Springs, MI 49104, USA*

¹⁴⁵*Università di Siena, I-53100 Siena, Italy*

¹⁴⁶*Trinity University, San Antonio, TX 78212, USA*

¹⁴⁷*Abilene Christian University, Abilene, TX 79699, USA*